ISSN 2523-6873

# Journal of Innovative Engineerin

Volume 7, Issue 20 — January — June — 2023

ECORFAN®

**Journal of Innovative Engineering**, Volume 7, Issue 20, January – June 2023, is a journal edited semestral by RINOE. La Raza Av. 1047 No.-Santa Ana, Cusco. Peru. Postcode: 11500, WEB: www.rinoe.org journal@rinoe.org. Editor in Chief: MIRANDA-TORRADO, Fernando. PhD. ISSN-2523-6873. Responsible for the latest update of this number RINOE Computer Unit. ESCAMILLA-BOUCHÁN, Imelda. PhD. LUNA SOTO, Vladimir. PhD. La Raza Av. 1047 No.-Santa Ana, Cusco-Peru. Postcode: 11500 last updated June 30, 2023.

# Journal of Innovative Engineering

## Definition of Research Journal

## Scientific Objectives

Support the international scientific community in its written production Science, Technology and Innovation in the Field of Engineering and Technology, in Subdisciplines Production systems design, product quality management, operations research, computer simulation, supply chains, quality certification, hydrometeorology.

ECORFAN-Mexico SC is a Scientific and Technological Company in contribution to the Human Resource training focused on the continuity in the critical analysis of International Research and is attached to CONAHCYT-RENIECYT number 1702902, its commitment is to disseminate research and contributions of the International Scientific Community, academic institutions, agencies and entities of the public and private sectors and contribute to the linking of researchers who carry out scientific activities, technological developments and training of specialized human resources with governments, companies and social organizations.

Encourage the interlocution of the International Scientific Community with other Study Centers in Mexico and abroad and promote a wide incorporation of academics, specialists and researchers to the publication in Science Structures of Autonomous Universities - State Public Universities - Federal IES - Polytechnic Universities - Technological Universities - Federal Technological Institutes - Normal Schools - Decentralized Technological Institutes - Intercultural Universities - S & T Councils - CONAHCYT Research Centers.

## Scope, Coverage and Audience

Journal of Innovative Engineering is a Research Journal edited by ECORFAN-Mexico S.C in its Holding with repository in Republic of Peru, is a scientific publication arbitrated and indexed with semester periods. It supports a wide range of contents that are evaluated by academic peers by the Double-Blind method, around subjects related to the theory and practice of Production systems design, product quality management, operations research, computer simulation, supply chains, quality certification, hydrometeorology with diverse approaches and perspectives , That contribute to the diffusion of the development of Science Technology and Innovation that allow the arguments related to the decision making and influence in the formulation of international policies in the Field of Engineering and Technology. The editorial horizon of ECORFAN-Mexico® extends beyond the academy and integrates other segments of research and analysis outside the scope, as long as they meet the requirements of rigorous argumentative and scientific, as well as addressing issues of general and current interest of the International Scientific Society.

## Editorial Board

## Arbitration Committee

**Assignment of Rights**

The sending of an Article to Journal of Innovative Engineering emanates the commitment of the author not to submit it simultaneously to the consideration of other series publications for it must complement the Originality Format for its Article.

The authors sign the Authorization Format for their Article to be disseminated by means that ECORFAN-Mexico, S.C. In its Holding Republic of Peru considers pertinent for disclosure and diffusion of its Article its Rights of Work.

**Declaration of Authorship**

Indicate the Name of Author and Coauthors at most in the participation of the Article and indicate in extensive the Institutional Affiliation indicating the Department.

Identify the Name of Author and Coauthors at most with the CVU Scholarship Number-PNPC or SNI-CONAHCYT- Indicating the Researcher Level and their Google Scholar Profile to verify their Citation Level and H index.

Identify the Name of Author and Coauthors at most in the Science and Technology Profiles widely accepted by the International Scientific Community ORC ID - Researcher ID Thomson - arXiv Author ID - PubMed Author ID - Open ID respectively.

Indicate the contact for correspondence to the Author (Mail and Telephone) and indicate the Researcher who contributes as the first Author of the Article.

**Plagiarism Detection**

All Articles will be tested by plagiarism software PLAGSCAN if a plagiarism level is detected Positive will not be sent to arbitration and will be rescinded of the reception of the Article notifying the Authors responsible, claiming that academic plagiarism is criminalized in the Penal Code.

**Arbitration Process**

All Articles will be evaluated by academic peers by the Double Blind method, the Arbitration Approval is a requirement for the Editorial Board to make a final decision that will be final in all cases. MARVID® is a derivative brand of ECORFAN® specialized in providing the expert evaluators all of them with Doctorate degree and distinction of International Researchers in the respective Councils of Science and Technology the counterpart of CONAHCYT for the chapters of America-Europe-Asia- Africa and Oceania. The identification of the authorship should only appear on a first removable page, in order to ensure that the Arbitration process is anonymous and covers the following stages: Identification of the Research Journal with its author occupation rate - Identification of Authors and Coauthors - Detection of plagiarism PLAGSCAN - Review of Formats of Authorization and Originality-Allocation to the Editorial Board- Allocation of the pair of Expert Arbitrators-Notification of Arbitration -Declaration of observations to the Author-Verification of Article Modified for Editing-Publication.

**Instructions for Scientific, Technological and Innovation Publication**

**Knowledge Area**

The works must be unpublished and refer to topics of Production systems design, product quality management, operations research, computer simulation, supply chains, quality certification, hydrometeorology and other topics related to Engineering and Technology.

## Presentation of Content

In the first article we present, *Design of experiments (DOE) of parts manufactured in 3D printers using composed filaments of PLA and Aluminum* by LÓPEZ-CORELLA, José Alejandro, HERNÁNDEZ-RUÍZ, Sergio Iván, VÁZQUEZ-CUEVAS, Ignacio Javier and NAVIDAD-LÓPEZ, Ruben Alejandro, with adscription in Instituto Tecnológico de Nogales, as the netx article we present, *Europium metal organic frameworks: Chemical and Optical properties* by SÁNCHEZ-FABILA, Barbara Michelle, LOERA-SERNA, Sandra and GARDUÑO-WILCHES, Ismael A., with adscription in Universidad Autónoma Metropolitana and CONACyT, as the netx article we present, *$Sn_3Sb_2S_6$ thin films for photovoltaic applications* by GONZALEZ-GARZA, Jorge Oswaldo, GARCÍA-GUILLEN, Grisel, RÍOS-RAMÍREZ, Bernardino and DE RAMÓN-CONDÉ, Andres, with adscription in Universidad Politécnica de García, as the last article we present, *Destructive Test in 3D Printing* by LERMA-GARCÍA, Miguel Angel, ROSALES-GALLEGOS, Israel Atzin, TUDÓN-MARTÍNEZ, Alberto and DOMÍNGUEZ-HERNÁNDEZ, Carlos Alberto, with adscription in Universidad Tecnológica de San Luis Potosí.

.

## Content

Article **Journal of Innovative Engineering**
June 2023 Vol.7 No.20 1-6

# Design of experiments (DOE) of parts manufactured in 3D printers using composed filaments of PLA and Aluminum

# Diseño de experimentos (DOE) de piezas fabricadas en impresoras 3D utilizando filamentos compuestos de PLA y Aluminio

LÓPEZ-CORELLA, José Alejandro†*, HERNÁNDEZ-RUÍZ, Sergio Iván, VÁZQUEZ-CUEVAS, Ignacio Javier and NAVIDAD-LÓPEZ, Ruben Alejandro

*Tecnológico Nacional de México/Instituto Tecnológico de Nogales*

ID 1st Author: *José Alejandro, López-Corella* / **ORC ID**: 0000-0001-5776-7665, **CVU CONAHCYT ID**: 551626

ID 1st Co-author: *Sergio Iván, Hernández-Ruíz*, / **ORC ID**: 0000-0001-6560-0101, **CVU CONAHCYT ID**: 105423

ID 2nd Co-author: *Ignacio Javier, Vázquez-Cuevas* / **ORC ID**: 0000-0001-6849-4463, **CVU CONAHCYT ID**: 478643

ID 3rd Co-author: *Ruben Alejandro, Navidad-López* / **ORC ID**: 0009-0006-8319-8834

**DOI**: 10.35429/JOIE.2023.20.7.1.6 Received March 27, 2023; Accepted June 30, 2023

**Abstract**

The Department of Mechanical Metal (Mechatronic Engineering) of the Technological Institute of Nogales was one of the first national degrees to offer in its study plans the specialty of plastic injection molding (IMCE-MIP-2017-01), with the eager to continue innovating and evolving in this area, we present the following research work, with which we experimented and generated knowledge to determine the mechanical properties of parts manufactured in 3D printers, with polymer composite materials (PLA) and metallic powders ( Aluminum). In the first place, the filament formed by a matrix of PLA and an ALUMINUM reinforcement was created, which was extruded in a molding machine manufactured inside in the molding laboratory of this Institute, taking as consideration that the reinforcing material in this case aluminum the following percentages will be 0% and 20%. Placing these filaments in a suitable printer for the manufacture of 3D parts with composite materials to which an analysis of experiments was performed to determine what percentage of composite material has better mechanical properties

**PLA Filament, Composite Material, Design of Experiments (DOE)**

**Resumen**

El departamento de Metal Mecánica (Ingeniería Mecatrónica) del Instituto Tecnológico de Nogales fue de las primeras licenciaturas a nivel nacional en ofrecer dentro de sus planes de estudio la especialidad de moldeo por inyección de plásticos (IMCE-MIP-2017-01), con el afán de continuar innovando y evolucionando en esta área, se presenta el siguiente trabajo de investigación, con el cual se experimentó y generó conocimiento para determinar las propiedades mecánicas de piezas fabricadas en impresoras 3D, con materiales compuestos de polímero (PLA) y polvos metálico (Aluminio). En primer lugar, se creó el filamento formado por una matriz de PLA y un refuerzo de ALUMINIO, el cual fue extruido en una máquina moldeadora fabricada dentro en el laboratorio de moldeo de este Instituto, tomando como consideración que el material de refuerzo en este caso aluminio serán los siguientes porcentajes 0% y 20%. Colocando estos filamentos en una impresora adecuada para la fabricación de piezas en 3D con materiales compuestos a las cuales se les realizó un análisis de experimentos para determinar qué porcentaje de material compuesto tiene mejores propiedades mecánicas.

**Filamento PLA, Material compuesto, diseño de experimentos (DOE)**

**Citation**: LÓPEZ-CORELLA, José Alejandro, HERNÁNDEZ-RUÍZ, Sergio Iván, VÁZQUEZ-CUEVAS, Ignacio Javier and NAVIDAD-LÓPEZ, Ruben Alejandro. Design of experiments (DOE) of parts manufactured in 3D printers using composed filaments of PLA and Aluminum. Journal of Innovative Engineering. 2023. 7-20: 1-6

*Correspondence to Author (e-mail: jose.lc@nogales.tecnm.mx)
† Researcher contributing as first Author.

 

## Introduction

Conventional manufacturing processes are based on the use of resources with a large capacity of control elements to achieve very high levels of precision and reliability. The use of computer systems in the design, manufacturing and simulation engineering phases of a product, in combination with other techniques based on mechatronics, have managed to raise production systems to high levels of efficiency Mesa María (2015). Within the manufacturing processes of a product, three groups of technologies can be distinguished, depending on the method of obtaining the required geometry:

– Conformative technologies: Molds or preforms are used to achieve the geometry of the part. This set encompasses all known molding techniques.

– Subtractive technologies: The specific geometry is obtained by removing material from a larger geometry. It includes techniques such as machining, EDM and cutting by water jet or laser.

– Additive technologies: geometry is obtained by adding material layer by layer according to a virtual 3D design, without resorting to molds and without removing material.

This research is focused on the use of additive technology, specifically 3D printing with composite materials, modifying the mechanical properties of the manufactured parts, generating knowledge that greatly contributes to the contribution of advantages in the field of education.

## State of the Art

At the Polytechnic University of Madrid, Technical School of Industrial Engineering, the aluminum castability study was carried out with models made in PLA by 3D printing, the objective of which is to obtain unique parts for prototyping or very small print runs per the casting process with lost models in polymers manufactured by 3D printing, a casting process basically consists of pouring liquid metal into a mold with the geometry of the part to be manufactured inside and its subsequent solidification and cooling.

To achieve this end, the traditional molding system (green molding and chemical molding) will be maintained. The main variant of the project is the replacement of the molds created from any material with the possibility of being machined (metal, wood, resins, waxes, among others) with the cost of tooling that entails and using 3D technology. In the study we proceed to the union of both technologies, 3D printing and the casting process, manufacturing a model in a polymer using a 3D printer. The manufacture of the models is carried out by the material deposition system from a coil Bustos Carolina (2016).

In the Department of Continuous Media Mechanics and Theory of Structures of the Higher Technical School of Engineering at the University of Seville, work was done on the development of an additive manufacturing system for composite materials, as well as the characterization of the material used. Said system is related to a 3D printer that allows the use of two types of materials: thermoplastic filament (nylon) and composite filament (fiberglass, carbon fiber and Kevlar). The novelty of the printer is the manufacture with fiber reinforcements, which allows obtaining parts with better rigidity and resistance properties than the usual ones obtained with printers for plastic materials Mesa María (2015).

In the Faculty of Biotechnology of the University of Liubliana in Slovenia in conjunction with the Faculty of Mechanical Engineering in Sarajevo, they are working on research related to the effect of the wood contained in the properties of the filaments used in 3D printing Mirko Kariz (2017).

## System Components

Polymer (PLA)

Polymers based on renewable or biodegradable resources are generating growing interest, both in society in general and in the plastics industry, as well as in the agricultural sector, since it would mean an outlet for their products towards different markets. Poly (lactic acid) PLA is a synthetic thermoplastic polymer from the family of alpha hydroxy acids or aliphatic polyesters derived 100% from renewable raw materials, which are produced from lactic acid Valero Manuel (2013).

ISSN 2523-6873

Lactic acid is produced by anaerobic fermentation of carbon-containing substrates, either pure (glucose, lactose) or impure (starch, mixtures) with bacteria and fungi. PLA molecules can be synthesized through a lactic acid condensation polymerization process at a temperature not less than 120 degrees Celsius. PLA is characterized by its good mechanical properties compared to other thermoplastic polymers (such as PET, the best-known thermoplastic polyester). PLA also has good barrier properties against odors and flavors, likewise it has high resistance to fats and oils, making it appropriate for packaging oils, dry and perishable products. PLA has been used in biomedical applications in drug-controlled release systems, thanks to its biodegradability. To improve the properties of PLA, it can be mixed with plasticizing agents, metals or other polymers.

Metallic powders

The metallic powders available for additive manufacturing are largely the same as those used in many areas of industrial application (such as: aerospace, automotive, medical devices, among others) Escorsa Enric (2017), such as: stainless steels, aluminum alloys, cobalt-chromium or nickel superalloys, pure titanium or titanium alloys, copper alloys, precious metals (gold, silver, platinum, palladium, among others), developments and current aluminum application patents are shown below : Anvil Semiconductors, uses aluminum (US2017018634A1) and Hamilton Sundstrand aluminum alloys and other metals (US2017016093A1); Hitachi (EP3118865A1) iron, aluminum and chrome alloys. UACJ Corp aluminum alloys that allow thermal bonding (EP13884783A).

## Methodology

As previously mentioned, PLA is a thermoplastic synthetic polymer derived from renewable raw materials that are produced from lactic acid. Its main advantages are that it is biodegradable, recyclable and compostable. In addition to saving energy since 25-55% less energy is required for its production compared to petroleum-based polymers Valero Manuel (2013). PLA is characterized because its mechanical properties are good compared to other thermoplastic polymers (such as PET).

In order to modify the mechanical properties of PLA, in this work it was mixed with aluminum metal powders and the process is described below.

Preparation and generation of the filament.

The research of the Faculty of Biotechnology of the University of Liubliana Slovenia Mirko Kariz (2017) was taken as a reference. In which a material with wood dust is manufactured, it began with the smallest combination 80 - 20 in which good results were not obtained, retaking this investigation and applying the Taguchi methodology of a $2^2$ Factorial design (see Table 1). The creation of the new composite materials has been carried out by means of the extrusion-composition of a filament with an approximate diameter of 1.75 mm extruded at a temperature of 175 °C, using 80 grams of PLA reinforced with Aluminum 20 metal powders as a base matrix. grams, for the generation of a composite material (see Figure 1).


**Figure 1** Mixture of PLA with metallic aluminum powder (80% PLA and 20% Al).
*Source: TecNM / ITN*

| | MA1(%) | MA2(%) | MA3(%) | MA4(%) |
|---|---|---|---|---|
| PLA | 100 | 80 | 90 | 95 |
| Aluminio | 0 | 20 | 10 | 5 |

**Table 1** Percentages of PLA and Aluminum
*Source: TecNM / ITN*

ISSN 2523-6873

Manufacture of the 3D part with the filament made up of PLA and Aluminum

The composite filament with the aluminum metallic powder was placed in the Flash Forge Creator Pro 3D printer for the manufacture (at a controlled temperature of 21°C) of the 3D part to which the tests described in the following section were performed. The printing parameters configured in the printer are the following:

– Resolution: Standard.
– Layer height: 0.18mm.
– Height of the first layer: 0.27mm.
– Filling density: 100%.
– Pattern density: Line.
– Printing speed: 60mm/s.
– Travel speed: 80mm/s.
– Extruder temperature: 180°C.
– Platform temperature: 50°C.

In Figure 2, you can see the image of the part modeled in SolidWorks and manufactured in the 3D printer to which the stress tests were applied.

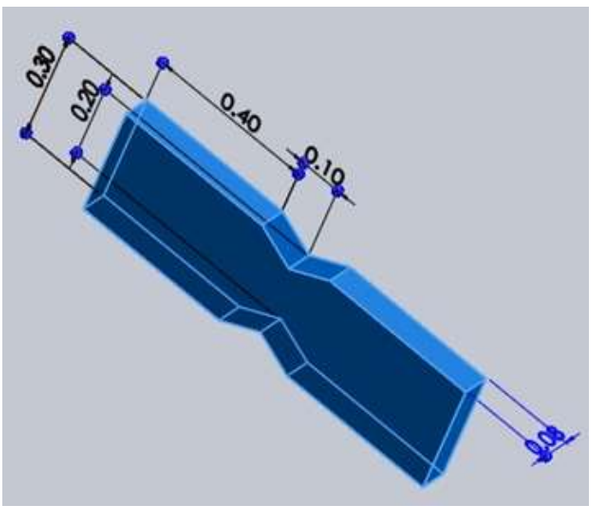


**Figure 2** Modeling of the part manufactured in the 3D printer with the composite material used for tension (inch units)
*Source: TecNM / ITN*

Figure 3 shows the image of the part modeled in SolidWorks and manufactured in the 3D printer to which the compression tests were applied.

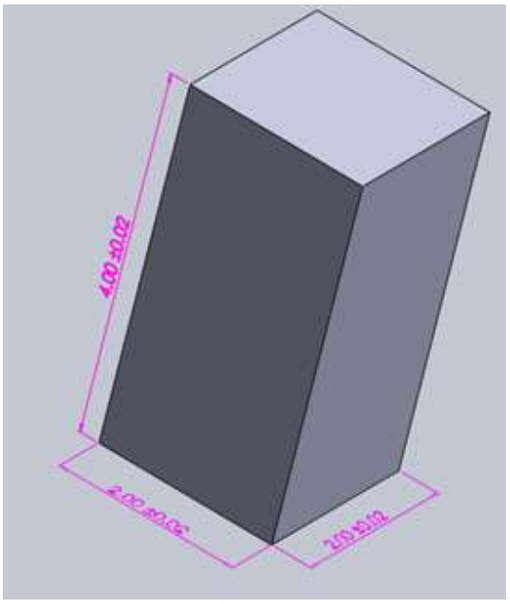

**Figure 3** Modeling of the part manufactured in the 3D printer with the composite material used for compression (inch units)
*Source: TecNM / ITN*

## Results

Tension and compression tests were carried out in a universal tension, bending and compression machine model: WDW-S5 (with traceability to CENAM and NIST) owned by the company Metrología y Pruebas S.A. de C.V. (MYPSA), as can be seen in Figure 4.

**Figure 4** Tension, bending and compression machine model: WDW-S5
*Source: MYPSA*

ISSN 2523-6873

Table 2 shows the result of the destructive tension test of 3 pieces created with pure PLA, the fracture point was in the center of the piece, which has a cross-sectional area of 0.016 in2 and the greatest effort was 6210 psi, on the specification sheet for this material gives us a maximum tensile strength of 7,000 psi.

| PLA puro (MA1) | | |
|---|---|---|
| P (LBF) | Area ($in^2$) | Esfuerzo (PSI) |
| 99.365578 | 0.016 | 6210.34863 |
| 87.67551 | 0.016 | 5479.71938 |
| 76.210251 | 0.016 | 4763.14069 |
| PLA-AL (MA2) | | |
| 76.43506 | 0.024 | 3184.79412 |
| 78.008723 | 0.024 | 3250.36346 |
| 76.210251 | 0.024 | 3175.42713 |
| PLA-AL (MA3) | | |
| 89.249173 | 0.016 | 5578.07331 |
| 59.799194 | 0.016 | 3737.44963 |
| 56.651868 | 0.016 | 3540.74175 |
| | | PLA-AL (MA4) |
| 94.41978 | 0.016 | 5901.23625 |
| 125.443422 | 0.016 | 7840.21388 |
| 84.5281842 | 0.016 | 5283.0115 |

**Table 2** PLA tension destructive test
*Source: Own Creation*

Tests were carried out with 3 pieces of PLA with Aluminum, in which the fracture point was in the clamping of the jaws, which has a cross-sectional area of 0.024 in2 and the maximum stress was 3250.36 psi, as can be seen in the Table 2 PLA-AL (MA2).

As can be seen, there was a degradation of the PLA and aluminum composite material; During the creation of the filament, in the printed pieces and the tension tests it was possible to observe that the pieces were very fragile.

Compression tests of pieces created as in Figure 3 were also carried out, in which they were printed according to the percentages in Table 1, the results of these destructive tests can be seen in Table 3, as can be seen as in the tension test there is a degradation of the material from the ultimate stress.

| **PLA puro (MA1)** | | |
|---|---|---|
| P (LBF) | Area ($in^2$) | Esfuerzo (PSI) |
| 334.066174 | 0.04 | 8351.65435 |
| 332.267702 | 0.04 | 8306.69255 |
| 335.415028 | 0.04 | 8385.3757 |
| **PLA puro (MA2)** | | |
| 314.282982 | 0.04 | 7857.07455 |
| 288.205138 | 0.04 | 7205.12845 |
| 326.422668 | 0.04 | 8160.5667 |
| **PLA puro (MA3)** | | |
| 348.903568 | 0.04 | 8722.5892 |
| 292.926127 | 0.04 | 7323.15318 |
| 229.529989 | 0.04 | 5738.24973 |
| **PLA puro (MA4)** | | |
| 333.616556 | 0.04 | 8340.4139 |
| 460.85845 | 0.04 | 11521.4613 |
| 339.911208 | 0.04 | 8497.7802 |

**Table 3** PLA compression destructive test
*Source: Own Creation*

## Acknowledgments

Thanks to TecNM for finance this work and the companies Metrology and Tests (MIPSA) and Badger Meter Mexico for their collaboration.

## Financing

Funding: This work has been funded by TecNM Support for Scientific and Technological Research in the Educational Programs of the Federal Technological Institutes and Centers. Code 6475.18-P

## Conclusions

Among the main objectives of this work is to generate knowledge in the area of composite materials and 3D printing, the tests carried out generated data that, when interpreted, we reached the following conclusions:

The filaments that were generated were 1.5-meter sections since the piece to be printed required that amount of material (1.1 m). The filaments made with aluminum powder when being processed we realized that they were more brittle than those of PLA alone. We came to the conclusion that it was due to an excess of reinforcing material (Aluminium), which functioned as a source of heat and degraded the material since the material's technical sheet gives us a melt temperature of 188 to 210 ℃, we handle it at 175 ℃ since We observed that the material was burning and coming out very liquid and must have a viscous consistency (melt temperature).

ISSN 2523-6873

In the tests carried out, the highest stress was 6,210 psi. The specification sheet for this material gives us a maximum tensile stress of 7,000 psi (PLA in pellets for plastic injection molding). As it can be seen, the data is not very far from the maximum tensile stress of the PLA specification sheet used (we do not have any reference in 3D printing), we consider that the degradation was due to the high amount of aluminum metal powder. In the future, it is intended to carry out the same tests with smaller amounts of aluminum metal powder and we are comparing tensile strength given by the manufacturer of polymer for plastic injection molding. We hope to have a reference for 3D printing.

**References**

Bustos Carolina (2016), "Estudio Colabilidad del Aluminio con Modelos Realizados en PLA por Impresión 3D", Universidad Politécnica de Madrid Escuela Técnica Superior de Ingenieros Industriales. Estudio de colabilidad de aluminio con modelos realizados en PLA por impresión 3D - Archivo Digital UPM

Escorsa Enric (2017), "Manufactura aditiva e impresión en 3D en 2017, Un vistazo a los desarrollos patentados", IALE Tecnología. Manufactura aditiva e impresión 3D en PDF Free Download (docplayer.es)

León Cabezas (2017), "Innovate functionalized monofilaments for 3D printing using fused deposition modeling for the toy indutry", Manufacturing Engineering Society International Conference 2017, MESIC 2017, Spain. main.pdf (sciencedirectassets.com)

Mesa María (2015), "Puesta a punto de un sistema de fabricación aditiva para materiales compuestos", Dep. Mecánica de medios continuos y teoría de estructuras Escuela Técnica Superior de Ingeniería Universidad de Sevilla. Puesta a punto de un sistema de fabricación aditiva para materiales compuestos (us.es)

Mirko Kariz(2017), "Effect of wood content in FDM filament on properties of 3D printer parts", Material today communications, 2352-4928/2017 Elsevier Ltd. Effect of wood content in FDM filament on properties of 3D printed parts - ScienceDirect

Valero Manuel (2013), "Biopolímeros: avances y perspectivas", Dyna, año 80, Nro. 181, pp. 171-180, Medellín, ISSN: 0012-7353. https://www.redalyc.org/articulo.oa?id=49628728019

ISSN 2523-6873

Article **Journal of Innovative Engineering**
June 2023 Vol.7 No.20 7-15

# Europium metal organic frameworks: Chemical and Optical properties

# Redes metal orgánicas de Europio: Propiedades Químicas y Ópticas

SÁNCHEZ-FABILA, Barbara Michelle†[1], LOERA-SERNA, Sandra[1] and GARDUÑO-WILCHES, Ismael A.[2]

[1]*Universidad Autónoma Metropolitana, Azcapotzalco, CDMX, Mexico.*
[2]*CONACyT/National Polytechnic Institute, Center for Research in Applied Science and Advanced Technology, CDMX, Mexico.*

1st Author: *Barbara Michelle, Sánchez-Fabila* / **ORC ID:** 0009-0009-5239-7787, **CVU CONAHCYT ID**: 1269497

1st Co-author: *Sandra, Loera-Serna* / **ORC ID:** 0000-0001-9562-3195, **CVU CONAHCYT ID**: 172467

2nd Co-author: *Ismael A. Garduño-Wilches* / **ORC ID:** 0000-0003-2261-0419, **CVU CONAHCYT ID**: 216873

**DOI**: 10.35429/JOIE.2023.20.7.7.15 Recibido 19 de March, 2023; Aceptado 30 de June, 2023

**Abstract**

This paper presents the results of synthesizing five metal-organic frameworks (MOFs) of europium with luminescent properties using a stirring methodology at room temperature. The materials were obtained using the organic linkers benzene dicarboxylic acid (BDC), benzene tricarboxylic acid (BTC), naphthalene dicarboxylic acid (NDC), amino benzene dicarboxylic acid (BDC-$NH_2$) and hydroxybenzene dicarboxylic acid (BDC-OH). XRD and FTIR determined structural and optical properties, and, for three of the materials, SEM. The MOFs obtained have a crystal size of the order of nanometers and presented characteristic functional groups of organic linkers. Optical properties were determined by luminescence spectroscopy, and emission and excitation spectra were obtained. The photoluminescence data of the MOFs showed that the organic linkers were useful for the energy transfer to the lanthanide ion (antenna effect). The material with the highest emission was $Eu_2BDC_3$, and the one with the lowest was $Eu_2(BDC\text{-}NH_2)_3$. The latter did not present a defined crystalline structure. The $Eu_2(BDC\text{-}NH_2)_3$ and $Eu_2(BDC\text{-}OH)_3$ structures suffered the loss of emission over time. The materials with the highest emission can be used as chemical sensors, cell tracers, and electronic components, including some of their applications.

**Metal-organic frameworks, Europium, Luminescence**

**Resumen**

En este proyecto se presentan los resultados de la síntesis de cinco redes metal-orgánicas (MOFs), de europio con propiedades luminiscentes, utilizando una metodología de agitación a temperatura ambiente. Los materiales fueron obtenidos usando los ligantes orgánicos ácido benceno-dicarboxílico (BDC), ácido benceno-tricarboxílico (BTC), ácido naftaleno-dicarboxílico (NDC), ácido amino benceno-dicarboxílico (BDC-$NH_2$) y ácido hidroxi benceno-dicarboxílico (BDC-OH). Las propiedades estructurales y ópticas se determinaron mediante DRX, FTIR y, para tres de los materiales, SEM. Las MOFs obtenidas tienen tamaño de cristal del orden de nanómetros y presentaron grupos funcionales característicos de los ligantes orgánicos. Las propiedades ópticas se determinaron mediante espectroscopia de luminiscencia y se obtuvieron los espectros de emisión y excitación. Los datos de fotoluminiscencia de las MOFs mostraron que los ligantes orgánicos resultaron ser útiles para la transferencia de energía al ion lantánido (efecto antena). El material con mayor emisión fue $Eu_2BDC_3$ y el de menor fue $Eu_2(BDC\text{-}NH_2)_3$, este último no presentó una estructura cristalina definida. Las estructuras $Eu_2(BDC\text{-}NH_2)_3$ y $Eu_2(BDC\text{-}OH)_3$, sufrieron la perdida de emisión con el paso del tiempo. Los materiales con mayor emisión pueden utilizarse como sensores químicos, trazadores celulares, en componentes electrónicos, por mencionar algunas de sus aplicaciones.

**Redes metal orgánicas, Europio, Luminiscencia**

**Citation:** SÁNCHEZ-FABILA, Barbara Michelle, LOERA-SERNA, Sandra and GARDUÑO-WILCHES, Ismael A. Europium metal organic frameworks: Chemical and Optical properties. Journal of Innovative Engineering. 2023. 7-20: 7-15

*Correspondence to Author (e-mail: sls@azc.uam.mx)
† Researcher contributing as first Author.

 

## Introduction

The incorporation of ions to a transition metal or a rare earth of the lanthanide family in MOFs is encouraging due to the possible benefits for the production of luminescent emission: the ligands maintain minimum distances between adjacent emitting ions, diminishing the effect of reabsorption of the emitted radiation, also known as *"quenching."* In addition, the ligands can function as energy absorption centers that later transfer it to the ions, exciting them and causing light emission. [Eliseeva & Bunzl, 2010]. In particular, aromatic molecules such as carboxylic acids can significantly help since their delocalized electrons and energy state density facilitate the energy absorption process [Jiang *et al*., 2001] through the antenna effect.

In this effect, the electron interacts and resonates with the incident electromagnetic radiation, facilitating its excitation to higher energy levels; the relaxation of these electrons can transfer energy to the metal ion, producing light emission. There is a wide variety of binder molecules of this type, for example benzene dicarboxylic acid (BDC), benzene dicarboxylic acid (BTC), naphthalene dicarboxylic acid (NDC), amino benzene dicarboxylic acid (BDC $-NH_2$) and hydroxybenzene-dicarboxylic acid (BDC-OH), which are aromatic molecules that are suitable for forming luminescent MOFs.

$Er^{2+}$ or $Eu^{3+}$ cations, as such, exhibit weak luminescence, although some peculiarities have been observed in nanoparticles [Yu *et al*., 2004]. One way to activate them is by inserting them into inorganic compounds or by forming compounds with organic binders that allow an energy transfer to the metal and a symmetry breaking, thus favoring an increase in emission power [Aubouy *et al*., 2006]. The most common coordination number of europium compounds is 8 [Chen *et al*., 1999].

There are few reports of work with MOFs with luminescent properties based on the $Eu^{3+}$ lanthanide ion [Habimana *et al*., 2016; Medina- Velazquéz *et al*., 2016; Mirhosseini *et al*.,2021]. In this sense, the synthesis commonly used to obtain these materials is solvothermal, and synthesis times range from days to months, except for microwave-assisted synthesis, which lasts 20 minutes.

Conventional synthesis methods for obtaining MOFs represent a problem due to energy requirements, which increase production costs, and the use of toxic and carcinogenic solvents such as dimethylformamide (DMF). Our research group has implemented a synthesis technique by stirring at room temperature, where MOFs with nanometric sizes are obtained. This work presents the results of the structural and optical properties of different europium MOFs using this methodology.

## Experimental development

### Materials

The reagents used in the synthesis of the MOFs were: hexahydrated europium chloride ($EuCl_3 \cdot 6H_2O$, 99%) 1,4- chloride benzene dicarboxylic acid (BDC, 98 %), 1,3,5-benzene acid tricarboxylic acid (BTC, 95%) and dimethyl,2-aminobenzene-1,4-dicarboxylate (BDC-$NH_2$, 90%), dimethyl-2,5-hydroxybenzene-1,4-dicarboxylate (BDC-OH, 99%) and naphthalene-2,6-dicarboxylic acid (NDC, 99%), all from Sigma-Aldrich brand. Solvents were absolute ethanol (99%) and deionized water.

### Synthesis of the MOFs

A solution containing 1 mmol of the organic binder in water and another 0.5 mmol of the europium salt in ethanol was prepared. Once dissolved, the Eu solution was added dropwise to the organic binder solution. The mixture was kept under magnetic stirring for 12 h at room temperature. The solid obtained was separated from the liquid by centrifugation and dried in an oven for 4 h at 100°C. The solid was ground in an agate mortar and stored for further characterization.

### Characterization of the MOFs

The MOFs were subjected to characterization tests; for the structural analysis, powder X-ray diffraction (XRD) was used, and the determination of the diffractograms was carried out using a Bruker Advance 8 brand diffractometer, at a step of 0.02 °(2θ) every 0.4 seconds. For analysis of functional groups, the characterization of the samples by infrared spectroscopy with Fourier transform (FT-IR), a Perkin-Elmer brand "Spectrum one" spectrophotometer was used, at a resolution of 1 $cm^{-1}$ and with an attenuated total reflectance (ATR) configuration.

ISSN 2523-6873

The morphological characteristics of the MOFs were studied using scanning electron microscopy (SEM) on a Jeol model JSM-6390LV microscope, and the atomic composition using a Voyager microanalysis system from Noran Instruments coupled to the microscope. The photoluminescent spectra obtained using the Edinburgh Instruments FS5 spectrofluorimeter equipment determined the luminescent properties. To get the excitation and emission spectra of photoluminescence, tablets were prepared with 100 mg of each sample.

## Results

### Structural analysis

The diffractogram Figure 1 compares the pattern reported for the structure of DyBTC ($H_2O$) DMF [Guo *et al*., 2006] with the pattern obtained for the EuBTC sample. The reported structure is a dysprosium-synthesized MOF and corresponds to a three-dimensional lattice with a $P4_322$ space group, with a basic building unit with 7 $Dy^{3+}$ ions coordinated to a BTC ligand. The network has 6 x 6 Å channels along the (0 0 1) plane, as observed in the structure of the diagram in Figure 1, and is obtained by synthesis in the presence of DMF (10 mL) and $HNO_3$ (6 M) at 60 °C for 7 days. The structure of DyBTC($H_2O$)DMF is isoreticular to that obtained in this project for EuBTC; the reported patterns have peaks at the same Bragg angles and with practically the same relative intensities.

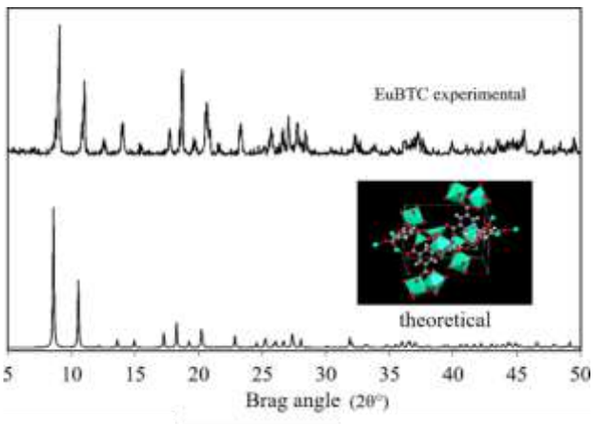


**Figure 1** Diffraction pattern of theoretical and experimental EuBTC

Figure 2 compares the XRD patterns of the materials synthesized with bidentate ligands and different functional groups, including all materials prepared with 1,4-benzene dicarboxylic precursors.

The theoretical $Eu_2BDC_3$ sample corresponds to a pattern reported by [Santos *et al*., 2017], with a solvothermal method at 120 ºC for 3 days. The lattice of this MOF has a space group P1 and is formed by the coordination of 8 $Eu^{3+}$ ions with 6 oxygens coming from the BDC ligands and 2 water molecules. Some missing peaks are observed in the XRD of the synthesized MOFs, indicating that the structure was not completely formed or had lower crystallinity than the reported lattice.

In the case of the sample with -$NH_2$, there is no defined pattern because the structure is not favored; it is probable that the -OH group generates interactions that tend to the structure, which does not occur for the amino group. The splitting energy can explain the difference between these two functional groups since the -OH is a low-field ligand in the chemical spectrum series, and the -$NH_2$ is a high field. This is attributed, among others, to the difference in electronegativity of the donor atoms. Since the formation of a coordination compound is sought, chemical factors that can change the donor nature of the carboxylic acids must be considered.

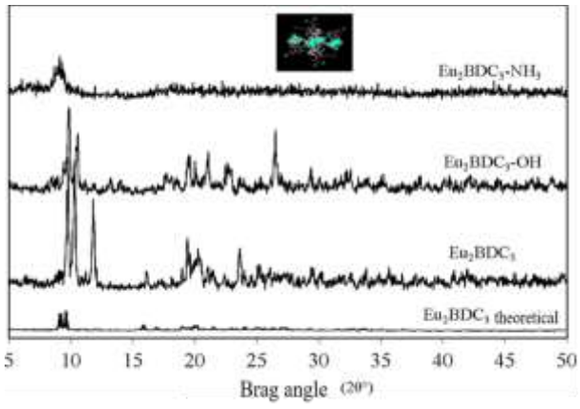


**Figure 2** Diffraction pattern of the MOFs**:** $Eu_2BDC_3$, $Eu_2(BDC\text{-}OH)_3$, $Eu_2(BDC\text{-}NH_2)_3$

Figure 3 compares the diffractograms of the experimental $Eu_2NDC_3$ MOFs with one reported for Nd and NDC [Wang *et al*., 201]. It is observed that the samples present peaks at the same Bragg angles. However, the diffractogram of the experimental MOF has less defined peaks, which is attributed to the low crystallinity of the material. In the work reported by Wang *et al*., a synthesis at room temperature was used, but this lasted several weeks. The metallic center they studied was neodymium, indicating an isoreticular structure was obtained.

ISSN 2523-6873

The Nd network comprises bi-dentate ligand chains and has a formula: $Nd(NDC)_{1.5}(H_2O)_2 \cdot 2DMA$. (DMA: dimethylacetamide).

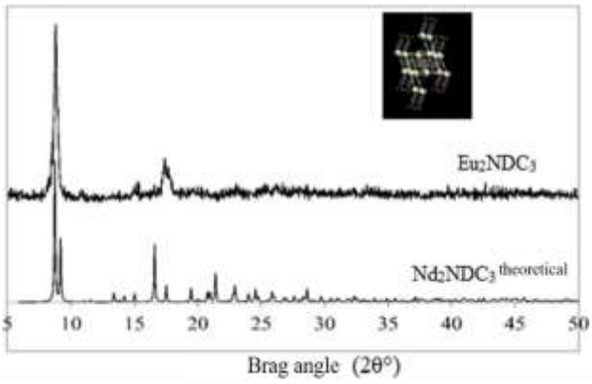


**Figure 3** Theoretical and experimental $Eu_2NDC_3$ diffraction pattern

## Crystal size

According to Debye's equation Scherrer (equation 1), the crystal size was determined for the samples EuBTC, $Eu_2BDC_3$, $Eu_2(BDC\text{-}OH)_3$, $Eu_2(BDC\text{-}NH_2)_3$ and $Eu_2NDC_3$ taking the value of 2Θ in the maximum peaks: 9.06, 9.75, 9.82, 9.09 and 7.7º, respectively. The results are described in Table 1.

$$D = \frac{k \cdot \lambda}{B cos cos\, \theta_B} \quad (1)$$

Where D is the crystal size, k is the Scherrer constant (value of 0.9), λ is the wavelength belonging to the line Cu kα(1.5406 Å), B is the width of the peak at half height (radians), and $\theta_B$ corresponds to the angle of the maximum peak in radians.

The crystal size for all the samples is in the range of 10-100 nm except the sample $Eu_2(BDC\text{-}NH_2)_3$, which presented a tiny crystal size, previously mentioned that it corresponds to the material that did not give a definite diffraction pattern. The sample with the largest crystal size is the MOF EuBTC with 49 nm. The change in size can be associated with the presence of donor groups in the organic binders. However, the presence of these groups can favor chemical interactions; for the formation of the structure, it is preferable not to have functional groups that interfere with the coordination of the metal and the oxygens of the ligand.

| Sample | D (nm) |
|---|---|
| EuBTC | 49 |
| $Eu_2BDC_3$ | 22 |
| $Eu_2(BDC\text{-}OH)_3$ | 16 |
| $Eu_2(BDC\text{-}NH_2)_3$ | 5 |
| $Eu_2NDC_3$ | 25 |

**Table 1** The crystal size of the MOFs.

## Analysis of functional groups

EuBTC, $Eu_2BDC_3$, $E_2(BDC\text{-}OH)_3$, $Eu_2(BDC\text{-}NH_2)_3$, and $Eu_2NDC_3$ are presented. As can be seen, in the spectra of the five samples, there are characteristic bands of the vibration of elongation of the metal-oxygen bond that would be Eu–O, located in the range of 400–560 $cm^{-1}$ [Lui *et al*., 2009], said band reveals that Eu atoms have successfully coordinated with carboxylate groups. In addition, the intense absorption at 3407 $cm^{-1}$ must be the –OH stretching vibration of water, indicating that water molecules act not only as the solvent but also as a reagent for forming the MOFs [Lui *et al*. 2009].

The bands located in the range of 1104–1110 $cm^{-1}$ are attributed to the doubling of the C–H bond in the plane of the ring [Silverstein *et al*., 1967]. All samples exhibit symmetric stretching vibrations of carboxylic groups in the range of 1590-1480 $cm^{-1}$ and symmetric vibrations centered at 1381 $cm^{-1}$ [Xu *et al*., 2011]. Particularly for the MOF $Eu_2NDC_3$, the band located at 1908 $cm^{-1}$ characteristic of the CN stretching vibration is presented [Hansen *et al*., 2022].

a)

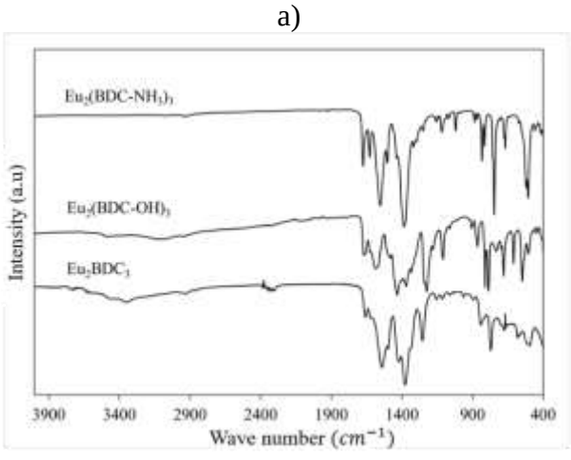


ISSN 2523-6873

b)

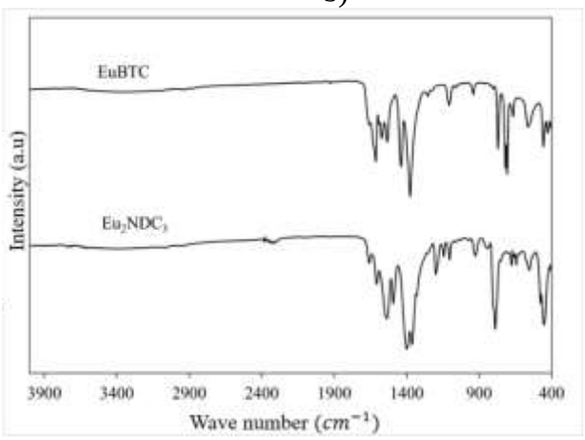


**Figure 4** IR spectra of a) $Eu_2BDC_3$, $Eu_2(BDC\text{-}OH)_3$ , $Eu_2(BDC\text{-}NH_2)_3$ and b) EuBTC and $Eu_2NDC_3$

## Morphology

Figure 5 shows the micrographs with 20,000 magnifications that could be obtained and correspond to the $Eu_2(BDC\text{-}OH)_3$, $Eu_2(BDC\text{-}NH_2)_3$, and $Eu_2NDC_3$ samples. In the $Eu_2(BDC\text{-}OH)_3$ material, aggregates of particles reaching 4.5 μm and small grains of lighter tonality and asymmetric morphology with a diameter of 0.5-0.8 μm are observed. In the $Eu_2(BDC\text{-}NH_2)_3$ sample, flower-shaped grains with a size of 7 μm are observed, whose petals are 2 μm long and 0.95 μm wide. Again, the aggregates are covered by tiny grains of 5-10 nm. In the sample $Eu_2NDC_3$, the same aggregates are seen (beginning to have a concentric formation), but with greater dispersion, the size is 3-4 μm, and the petal-shaped crystals are 1.5 μm long and 0.6 μm wide. These formations have been previously observed in microwave-obtained europium MOFs [Garduño-Wilches *et al.*, 2021].

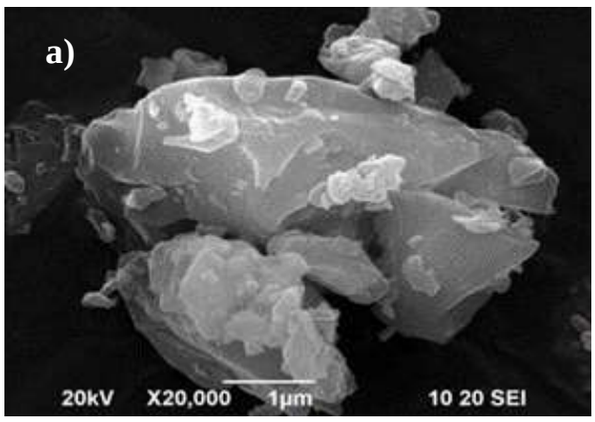


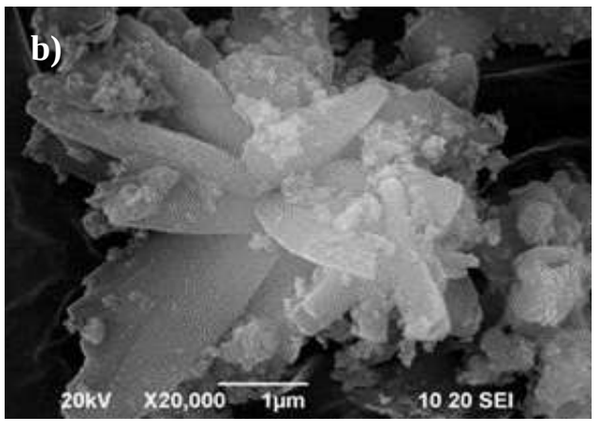


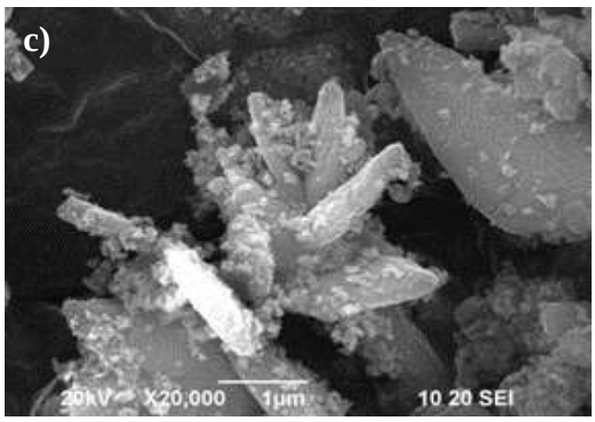


**Figure 5** Micrographs of a) $Eu_2(BDC\text{-}OH)_3$, b) $Eu_2(BDC\text{-}NH_2)_3$ and c) $Eu_2NDC_3$.

## Luminescent properties

The luminescent properties of the materials are described with the excitation and emission spectra to know the influence of the organic ligand (LO) on the lanthanide ion ($Ln^{3+}$), which are the components of the MOFs synthesized in this work.

## Emission spectra

Figure 6 shows the emission spectra of $Eu_2BDC_3$, $Eu_2$ $(BDC\text{-}OH)_3$, $Eu_2(BDC\text{-}NH_2)_3$ powders. The excitation wavelengths were set at 305 and 348 nm to obtain these spectra, respectively. In the spectrum of the MOF-$Eu_2BDC_3$, the 4 characteristic emission peaks of the transitions between the electronic energy states of the europium ion are shown. They are $5D_{0\ J} \rightarrow 7F_{,}$ where J= 1, 2, 3 and 4 [Han *et al.*, 2017] are located at 591, 617, 652, and 700 nm, respectively. It should be noted that the two remaining MOFs do not present a very strong intensity in the 4 transition states.

ISSN 2523-6873

It is observed that the highest intensity peak for the three samples is located between 600 and 630 nm, so the samples present an intense red emission. Differences in the bands of the MOFs were identified: $Eu_2(BDC\text{-}OH)_3$, $Eu_2(BDC\text{-}NH_2)_3$. The light emission of the sample $E_2BDC_3$ is the one with the highest intensity; the remaining two are of lower intensity, and its band in the $5D_0 \rightarrow 7F_2$ transition state presents two peaks, which is attributed to the splitting of this transition state, in addition, the change in intensity of this can be attributed to the $NH_2$ and OH groups, which modify the network. Considering that these samples in the DXR spectra present shorter interplanar distances, their crystal size is also smaller; this effect on the crystal is affected by the luminescence intensity they emit.

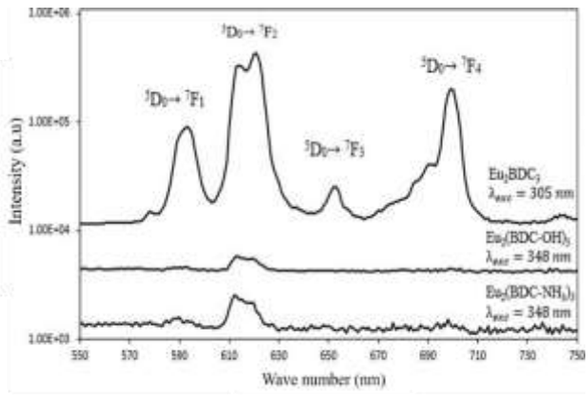


**Figure 6** Emission spectra of $Eu_2BDC_3$, $Eu_2$ (BDC- OH)$_3$, $Eu_2$ (BDC-$NH_2$)$_3$

Figure 7 presents the emission spectrum of $Eu_2BDC_3$, EuBTC, and $Eu_2NDC_3$, monitored with a 305 and 348 nm wavelength, respectively. It is observed that the three MOFs show the four typical transition states of $Eu^{3+}$ and an emission wavelength of 600-630 nm, where the MOF $Eu_2BDC_3$ presents the highest intensity, 105, followed by EuBTC and $Eu_2ND_3$ with an intensity of 104, where the MOF $Eu_2NDC_3$ is the one with the lowest intensity.

The emission intensity bands of $Eu_2BD_3$ and $Eu_2NDC_3$ show two different intensities in the $5D_0 \rightarrow 7F_2$ transition state, similar to the previous MOFs. These differ in emission intensity due to the depopulation of this state because they have a difference in the number of aromatic rings.

In the case of the EuBTC, the number of rings is the same as in the MOF $Eu_2BDC_3$. However, the number and positioning of the carboxylate groups will influence the antenna effect between them to impact the emission capacity.

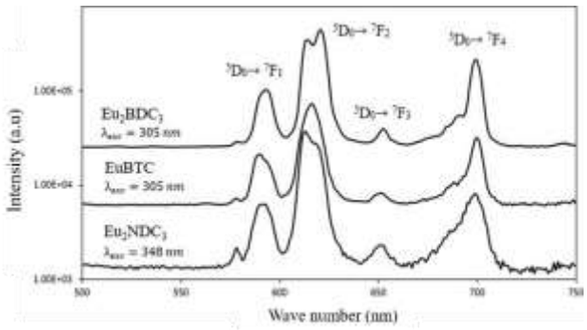


**Figure 7** Emission spectra of $Eu_2BDC_3$, EuBTC, and $Eu_2NDC_3$.

## Excitation spectra

The excitation spectra obtained from the samples $Eu_2$ (BDC)$_3$, $Eu_2(BDC\text{-}OH)_3$, and $Eu_2(BDC\text{-}NH_2)_3$, with emission wavelengths at 619 and 613 nm, respectively, are presented in Figure 8. A broad absorption band of the excitation energy is observed in the interval of wavelengths of 307 and 350 nm, respectively.

The excitation spectrum of $Eu_2$ (BDC)$_3$, Figure 8, shows a broad band from 307 to 333 nm and an absorption band at 330 nm, strongly related to the energy transfer between the aromatic rings in the organic phase. Of the MOF and the $Eu^{3+}$ ions (antenna effect), however, for the MOFs $Eu_2$ (BDC-OH)$_3$ and $Eu_2(BDC\text{-}NH_2)_3$, this band is shifted to a range of 357 to 370 nm, which is attributed to the functional groups $NH_2$ and OH.

The shift of the absorption bands of the MOFs to the UV spectrum greatly potentiates its implementation in biomedical applications. However, mediations were carried out after 1 month of the synthesis and previous studies, and the emission capacity in these networks was lost.

ISSN 2523-6873

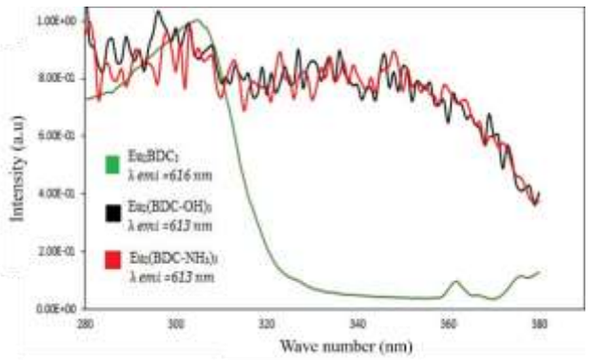


**Figure 8** Excitation spectra of $Eu_2(BDC)_3$, $Eu_2(BDC\text{-}OH)_3$ and $Eu_2(BDC\text{-}NH_2)_3$

The excitation spectrum of $Eu_2(BDC)_3$ and EuBTC is represented in Figure 8; the similarity in their patterns is observed. However, their absorption band differs; EuBTC is 300 nm, and $Eu_2(BDC)_3$ is 310 nm. Unlike the $Eu_2NDC_3$ (Figure 9) in which this band appears at 350 nm, which is strongly related to the energy transfer between the aromatic rings present in the organic phase of the MOF, in this case, it is naphthalene—and $Eu^{3+}$ ions (antenna effect).

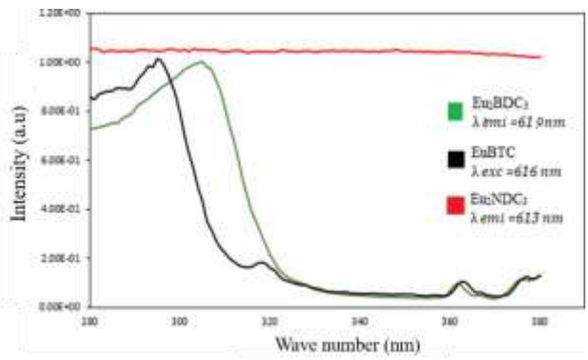


**Figure 9** Excitation photoluminescence spectra of $Eu_2BDC_3$, EuBTC and $Eu_2NDC_3$

The results from the photoluminescence spectra demonstrate an energy transfer between the organic ligand and the lanthanide ion. It is reasonable to conclude that a process of absorption and transmission of energy from the aromatic rings of the benzoate groups produces the emission of the $Eu^{3+}$ ions. In this luminescence process, the excitation energy is selective for the aromatic rings of the benzoate since the emitting levels of the $Eu^{3+}$ will be populated through the mechanism of sensitization of the excited state of the benzoate groups where these are working as an antenna since it is the molecule that absorbs the excitation energy and transfers it to the activating ions of the lanthanide series.

**Acknowledgment**

To the UAM Azcapotzalco, for the facilities to carry out this work.

**Financing**

Funding: This work has been funded by CONAHCYT [project CB A-S1-31186].

**Conclusions**

In this work, five different metal-organic networks based on the europium lanthanide ion were synthesized, with the organic ligands (BDC, BDC-OH, $BDC\text{-}NH_2$, BTC, and NDC) obtained by a synthesis method at room temperature, which turned out to be favorable compared to the most reported technique (solvothermal), mainly due to the reduction of reaction times, in addition to not using carcinogenic or harmful solvents for health and the environment. However, it was impossible to obtain a crystalline structure for the material synthesized with $BDC\text{-}NH_2$, which is attributed to the nucleophilicity of the functional group.

The photoluminescence data of the $Eu^{3+}$ complex showed that the organic ligands turned out to be helpful for the energy transfer of the lanthanide ion, because the organic ligands present the ability to transfer the appropriate and sufficient energy to the $Eu^{3+}$ ions, thanks to the mechanism of excitation that takes place in these elements, which is known as the antenna effect.

This study proposes a strategy to increase the luminescence intensity of MOFs by up to two orders of magnitude when treating them with different organic ligands, due to the presence of different numbers of functional groups, such as carboxylates, alcohols, aminos, and aromatic rings. that impact the properties of the MOFs; crystalline structure, grain size, morphology and emission intensity.

The samples $Eu_2(BDC\text{-}OH)_3$ and $Eu_2(BDC\text{-}NH_2)_3$ showed the ones with the lowest luminescence emission and a decay in this property over time. However, the energy they require to be excited is very favorable, since the wavelength is in the visible spectrum, and they are promising for their use in biomedical applications.

ISSN 2523-6873

Similar case for the MOF of $Eu_2NDC_3$, which presents an intense emission and because the ligand has two aromatic rings and allowed the excitation wavelength to be covered in the visible spectrum.

The MOFs with the highest luminescent intensity of exponential order 105 are the MOFs $E_2BDC_3$ and EuBTC, being the sample $Eu_2BD_3$ the MOF with the best luminescent properties, which were attributed to the presence of different organic compounds in each of them.

**References**

Aubouy, L., De la Varga, M., Bautista, L., Briz, A., de la Fuente, M., Garcia, O., De la Varga, M, Tzvetkova, M., & Parra, J. (2006). Europio: Naturaleza, luminiscencia y aplicaciones. In Anales de la Real Sociedad Española de Química (No. 4, pp. 40-45). *Real Sociedad Española de Química*. URL: https://docplayer.es/41178449-Europio-naturaleza-luminiscencia-y-aplicaciones.html

Chen, XF, Zhu, XH, Xu, YH, Raj, SSS, Öztürk, S., Fun, HK, Ma, J., & You, X. Z. (1999). Triboluminescence and crystal structures of non-ionic europium complexes. *Journal of Materials Chemistry*, 9(11), 2919-2922. DOI: 10.1039/A904411F. URL:https://pubs.rsc.org/en/content/articlehtml/1999/jm/a904411f

Eliseeva, SV, & Bunzli, JCG (2010). Lanthanide luminescence for functional materials and bio-sciences. *Chemical Society Reviews*, 39(1), 189-227. DOI: 10.1039/B905604C. URL:https://pubs.rsc.org/en/content/articlehtml/1999/jm/a904411f

Garduño-Wilches, IA, Alarcón -Flores, G., Carro-Gastélum, A., Carmona-Téllez, S., Aguilar- Frutis, MA, & Loera-Serna, S. (2021). Enhanced photoluminescence quantum yield of terbium nano-MOFs synthesized by microwave assisted solvothermal method. *Nano-Structures & Nano-Objects*, 26, 100736. DOI: 10.1016/j.nanoso.2021.100736. URL:https://www.sciencedirect.com/science/article/abs/pii/S2352507X21000378

Guo, X., Zhu, G., Li, Z., Sun, F., Yang, Z., & Qiu, S. (2006). A lanthanide metal–organic framework with high thermal stability and available Lewis-acid metal sites. *Chemical Communications*, (30), 3172-3174. DOI: 10.1039/B605428E. URL:https://pubs.rsc.org/en/content/articlelanding/2006/cc/b605428e/unauth

Habimana, F., Huo, Y., Jiang, S., & Ji, S. (2016). Synthesis of europium metal–organic framework (Eu-MOF) and its performance in adsorptive desulfurization. *Adsorption*, 22(8), 1147-1155. DOI: 10.1007/s10450-016-9838-1 URL:https://link.springer.com/article/10.1007/s10450-016-9838-1

Han, J., Zhang, S., Wei, Q., Xie , G., & Chen, S. (2017). Photoluminescence Properties of Lanthanide-Organic Frameworks ( LnOFs ) with Thiophene-2, 5-Dicarboxylate and Acetate. *Zeitschrift fur anorganische und allgemeine Chemie*, 643(13), 850-857. DOI: 10.1002/zaac.201700060. URL:https://onlinelibrary.wiley.com/doi/abs/10.1002/zaac.201700060

Hansen, PA, Svendsen, J., Nesteng, H., & Nilsen, O. (2022). Aromatic sensitizers in luminescent hybrid films. *RSC advances*, 12(28), 18063-18071. DOI: 10.1039/d2ra03360g. URL:https://pubs.rsc.org/en/content/articlehtml/2022/ra/d2ra03360g

Jiang, X., Jen, AKY, Huang, D., Phelan, GD, Londergan, TM, & Dalton, LR (2001). The effect of ligand conjugation length on europium complex performance in light-emitting diodes. *Synthetic metals*, 125(3), 331-336. DOI: 10.1016/S0379-6779(01)00482-9. URL:https://www.sciencedirect.com/science/article/abs/pii/S0379677901004829

Liu, K., You, H., Zheng, Y., Jia, G., Zhang, L., Huang, Y., Yang, M., Song, Y. & Zhang, H. (2009). Facile shape-controlled synthesis of luminescent europium benzene-1, 3, 5-tricarboxylate architectures at room temperature. *Crystal Engineering Communication*, 11(12), 2622-2628. DOI: 10.1039/b905924p. URL:https://pubs.rsc.org/en/content/articlelanding/2009/ce/b905924p/unauth

ISSN 2523-6873

Mirhosseini, H., Shamspur, T., Mostafavi , A., & Sargazi , G. (2021). A novel ultrasonic reverse micelle-assisted electrospun efficient route for Eu-MOF and Eu-MOF/CA composite nanofibers: a high-performance photocatalytic treatment for removal of BG pollutant. *environmental Science and Pollution Research*, 28(4), 4317-4328. DOI: 10.1007/s11356-020-10746-8. URL: https://link.springer.com/article/10.1007/s11356-020-10746-8

Medina- Velazquez, DY, Alejandre-Zuniga, BY, Loera-Serna, S., Ortiz, EM, Morales- Ramirez, ADJ, Garfias- Garcia, E., García-Murillo A. & Falcony, C. (2016). An alkaline one-pot reaction to synthesize luminescent Eu-BTC MOF nanorods, highly pure and water-insoluble, under room conditions. *Journal of Nanoparticle Research*, 18(12), 1-10. DOI: 10.1007/s11051-016-3593-9 URL: https://link.springer.com/article/10.1007/s11051-016-3593-9

Santos, GDC, Barros, AL, de Oliveira, CA, da Luz, LL, da Silva, FF, Demets , GJF, & Alves Júnior, S. (2017). New composites LnBDC @ AC and CB [6]@AC: from design toward selective adsorption of methylene blue or methyl orange. *Plos one*, 12(1), e0170026. DOI: 0.1371/journal.pone.0170026. URL: https://journals.plos.org/plosone/article?id=10.1371/journal.pone.0170026

Silverstein R., G. Clayton Bassler. 1967. *Spectrometric Identification of Organic Compounds*. Second edition, John Wiley and Sons, Inc. (Silverstein *et al*. 1967). URL: https://doi.org/10.1021/ed039p546

Wang, CC, Yeh, CT, Ke, SY, Cheng, YT, Yang, CC, Lee, GH, Changc C. & Sheu ,H. S. (2015). Assembly of three Nd (III) 2, 6-naphthalenedicarboxylates (ndc 2−) 3D coordination polymers based on various secondary building units (SBUs): structural diversity and gas sorption properties. *RSC advances*, 5(112), 92378-92386. DOI: 10.1039/C5RA10799G. URL : https://pubs.rsc.org/en/content/articlelanding/2015/ra/c5ra10799g/unauth

Xu, B., Guo, H., Wang, S., Li, Y., Zhang, H., & Liu, C. (2012). Solvothermal synthesis of luminescent Eu (BTC) (H 2 O) DMF hierarchical architectures. *Crystal Engineering Communication*, 14(8), 2914-2919. DOI: 10.1039/C2CE06572J. URL: https://pubs.rsc.org/en/content/articlelanding/2012/ce/c2ce06572j/unauth

Yu, L., Song, H., Lu, S., Liu, Z., Yang, L., & Kong, X. (2004). Luminescent properties of LaPO4: Eu nanoparticles and nanowires. *The Journal of Physical Chemistry B*, 108(43), 16697-16702. DOI: 10.1021/jp047688c. URL: https://pubs.acs.org/doi/abs/10.1021/jp047688c

ISSN 2523-6873

Article **Journal of Innovative Engineering**
June 2023 Vol.7 No.20 16-21

# $Sn_3Sb_2S_6$ thin films for photovoltaic applications

# Películas delgadas de $Sn_3Sb_2S_6$ para aplicaciones fotovoltaicas

GONZALEZ-GARZA, Jorge Oswaldo†*, GARCÍA-GUILLEN, Grisel, RÍOS-RAMÍREZ, Bernardino and DE RAMÓN-CONDÉ, Andres

*Universidad Politécnica de García, García, Nuevo León, México*

ID 1st Author: *Jorge Oswaldo, González Garza* / **ORC ID:** 0000-0002-9821-6947, **CVU CONAHCYT ID:** 248626

ID 1st Co-author: *Grisel, García-Guillen* / **ORC ID:** 0000-0002-5919-7755, **CVU CONAHCYT ID:** 297209

ID 2nd Co-author: *Bernardino, Ríos-Ramírez* / **ORC ID:** 0009-0007-6254-1223, **CVU CONAHCYT ID:** 329047

ID 3rd Co-author: *Andres, De Ramón-Condé* / **ORC ID:** 0009-0007-6653-7563, **CVU CONAHCYT ID:** 1289366

**DOI**: 10.35429/JOIE.2022.20.7.16.21 Received March 13, 2023; Accepted June 30, 2023

**Abstract**

Tin antimony sulfide semiconductor thin films have been extensively investigated due to their potential application as absorber in thin films solar cells, to convert solar radiation into electricity (A. Gassoumi, 2011; A. Larbi, 2014; Auttasit Tubtimtae, 2021; D. Abdelkader, 2014; N. Ali, 2015; Nisar Ali S. H., 2013a; Nisar Ali S. H., 2013b; Sebin Devasia, 2020); this is due to the excellent optoelectronic properties and due to abundance of the constituent elements on the earth crust and low toxicity. In this research we studied the effect of heat treatment temperature on the formation and optoelectronic properties of $Sn_3Sb_2S_6$ thin films prepared by the heating of multilayers glass/ $SnS/Sb_2S_3$ chemically deposited, the results show the formation of the ternary phase at temperatures above 250 °C, increasing the crystallinity of the phase at 325 °C. $Sn_3Sb_2S_6$ thin films show an indirect optical transition with band gaps around 1 eV, and absorption coefficient ~ $10^5$ $cm^{-1}$ in the visible range. $Sn_3Sb_2S_6$ thin films show conductivities in the range of $10^{-7}$ – $10^{-6}$ $Wcm^{-1}$, showing an increase in conductivity as the temperature increased. The good optoelectronic properties of this material make it suitable for photovoltaic applications.

**Optoelectronic, Semiconductor, Properties**

**Resumen**

Las películas delgadas de materiales semiconductores de la familia de sulfuro de antimonio estaño han sido objeto de investigación debido a su potencial aplicación como absorbedor en celdas solares de película delgada, para la generación de electricidad a partir de la radiación solar (A. Gassoumi, 2011; A. Larbi, 2014; Auttasit Tubtimtae, 2021; D. Abdelkader, 2014; N. Ali, 2015; Nisar Ali S. H., 2013a; Nisar Ali S. H., 2013b; Sebin Devasia, 2020); esto debido a sus excelentes propiedades optoelectrónicas y a que sus elementos constituyentes son abundantes en la corteza terrestre y son de baja toxicidad. En esta investigación se estudió el efecto de la temperatura de tratamiento térmico en la formación y propiedades optoelectrónicas de películas delgadas de $Sn_3Sb_2S_6$ preparadas mediante el calentamiento de multicapas de vidrio/$SnS/Sb_2S_3$ preparadas mediante la técnica de baño químico, los resultados muestran la formación de la fase ternaria a temperaturas superiores a 250 °C, aumentando su cristalinidad a una temperatura de 325 °C. Las películas delgadas de $Sn_3Sb_2S_6$ muestran una transición óptica indirecta con brechas de energía cercanas a 1 eV, y coeficientes de absorción ~ $10^5$ $cm^{-1}$ en el rango del espectro visible. Las películas delgadas de $Sn_3Sb_2S_6$ muestran conductividades de $10^{-7}$ – $10^{-6}$ $Wcm^{-1}$, observándose un incremento en la conductividad conforme aumenta la temperatura. Las buenas propiedades optoelectrónicas obtenidas hacen que este material sea prometedor para aplicaciones fotovoltaicas.

**Optoelectrónico, Semiconductor, Propiedades**

**Citation:** GONZALEZ-GARZA, Jorge Oswaldo, GARCÍA-GUILLEN, Grisel, RÍOS-RAMÍREZ, Bernardino and DE RAMÓN-CONDÉ, Andres. $Sn_3Sb_2S_6$ thin films for photovoltaic applications. Journal of Innovative Engineering. 2023. 7-20: 16-21

*Correspondence to Author (e-mail: jorge.gonzalez@upgarcia.edu.mx)
† Researcher contributing as first Author.

 

## 1. Introduction

Thin film solar cell (TFSC) technology is based on copper indium gallium selenium (CIGS) and CdTe absorber materials, which have demonstrated the best efficiency conversion of sunlight into electricity in TFSC technology; efficiencies of 22.6% and 22.1%, have been reported for CIGS (Taoufik Chargui, 2023) and CdTe (E.I. Emon, 2023), respectively. The main drawback with these absorber materials is the scarcity of indium and gallium, and the toxicity of cadmium. In that fact, new absorber materials are being extensively studied, focusing on the availability of the constituent elements and low toxicity (Aiswarya Nadukkandy, 2023; Jiayou Xue, 2023). Ternary compounds base on tin antimony sulfide (TAS) sulfosalts family are good candidates as absorber materials for thin films solar cell technology.

The chemistry of this sulfosalt family is $A_xB_yX_z$, where A is the metallic atom such as tin ($Sn^{2+}$, $Sn^{4+}$), Iron ($Fe^{2+}$), etc. B corresponds to the metallic atoms like Antimony ($Sb^{3+}$), Arsenic ($As^{3+}$), and X is the anion such as Sulfur ($S^{-2}$), Selenium ($Se^{2-}$) (Sebin Devasia, 2020). Abdelkader *et al*. prepared $SnSb_4S_7$, $Sn_2Sb_6S_{11}$, $SnSb_2S_4$, $Sn_4Sb_6S_{13}$, $Sn_2Sb_2S_5$ and $Sn_3Sb_2S_6$ thin films by thermal evaporation of the corresponding $Sn_xSb_yS_z$ powders; the powders were obtained by crushing $Sn_xSb_yS_z$ ingots prepared by the Bridgman method. The optical properties of the TAS thin films were analyzed, the films showed high absorption coefficients in the visible region around $10^5$ $cm^{-1}$, direct and indirect optical transitions, with band gaps in the range of 1.37 – 1.87 eV, depending on the chemical composition (D. Abdelkader, 2014). Bindu *et al*. prepared $Sn_6Sb_{10}S_{21}$ by heating chemically deposited multilayers of $Sb_2S_3$/SnS in vacuum; the thin films showed band gaps 1.26 – 1.45 eV, and high absorption coefficient $10^5$ $cm^{-1}$, moreover, $Sn_6Sb_{10}S_{21}$ thin films were incorporated as absorber in a photovoltaic structure, the obtained cell parameter were: $V_{oc}$ = 409 mV, $J_{sc}$ = 1.46 mA/$cm^2$, and FF = 0.25 (Sebin Devasia, 2020).

To our knowledge there are no reports of the preparation $Sn_3Sb_2S_6$ by heating multilayers of SnS/$Sb_2S_3$ deposited by chemical bath deposition. The findings in this work are relevant and can contribute to the development of photovoltaic structures using this material as absorber.

## 2. Methods

### 2.1 Deposition of SnS thin films

SnS thin films were deposited on clean glass Corning substrates, that, previously to deposition, were washed with neutral detergent and rinsed with distilled water. For the deposition, 1 g of $SnCl_2$:$2H_2O$ was dissolved in 5 ml of acetone, and to this solution 12 ml of triethanolamine (3.7M) was added, followed by 65 ml of deionized water, 8 ml of thioacetamide (1M), and 10 ml of $NH_3$ (4M) (David Avellaneda, 2007). Cleaned glass substrates were placed vertically on a 100 ml beaker and the temperature was maintained at 40 °C for 20 h. Uniform SnS thin films of ~ 500 nm were obtained; thickness was measured using a Alpha-Step D-600 Stylus profiler.

### 2.2 Deposition of $Sb_2S_3$ thin films

On the glass/SnS structure $Sb_2S_3$ thin films were deposited. For this, 650 mg of $SbCl_3$ was dissolved in 2.5 ml of acetone in a 100 ml beaker, and then 25 ml of 1 molar $Na_2S_2O_3$ solution was added followed by 72.5 ml of precooled distilled water at 10 °C, the final solution was mixed for 30 s, and glass/SnS simples were placed vertically in the beaker for 4.5 h and maintained at 10 °C (J.O. Gonzalez, 2014), two consecutive deposits were done.

### 2.3 Heat treatment of glass/SnS/$Sb_2S_3$ multilayers

The glass/SnS/$Sb_2S_3$ multilayers were heated in a conventional non-vacuum furnace at 100°C, 150 °C, 200 °C, 250 °C, 300 °C and 325 °C in air for 1 h.

## 3. Results and Discussion

XRD diffractograms for the glass/SnS/$Sb_2S_3$ multilayers heated at 100 °C, 150 °C, 200 °C, 250 °C, 300 °C and 325 °C in air are shown in graphic 1. At 100 °C, 150 °C and 200 °C the samples show the formation of two phases, SnS and $Sn_2S_3$. Peaks at 2θ of 28.55° and 30.52° are indexed to the planes (1 1 2) and (0 1 3), respectively, and correspond to Ottemannite phase (Card. No. 9011236). A peak at 2θ = 31.54 ° corresponds to the plane (1 3 0) of the phase SnS (Card. No. 9008785).

ISSN 2523-6873

It is evident that at temperatures below 200 °C no diffusion of the Sn, S and Sb constituent elements occurs for the formation of the ternary $Sn_3Sb_2S_6$ thin films.

At a temperature of 250 °C we observe the formation of two additional phases, named $Sb_2S_3$ and $Sn_3Sb_2S_6$. Two peaks at 2θ of 24.94° and 27.62°, are indexed to the planes (1 1 4) and (4 0 9) and corresponds to the ternary phase of $Sn_3Sb_2S_6$ (Card. No. 1541641). The formation of the ternary phase $Sn_3Sb_2S_6$ is explained as follows: as the temperature increases the Sn, Sb and S species diffuses between SnS and $Sb_2S_3$ layers, the species diffuses from the higher concentration region to the lower concentration region and react according to the following proposed reactions: $3SnS + Sb_2S_3 \rightarrow Sn_3Sb_2S_6$ and $3Sn_2S_3 + 2Sb_2S_3 \rightarrow 2Sn_3Sb_2S_6 + 3S\uparrow$ (g). The intensity of the $Sn_3Sb_2S_6$´s peaks is low, indicating low crystallinity, additionally, it is evident unreacted SnS, $Sn_2S_3$ and $Sb_2S_3$ (denoted as "#" in the diffractogram, card. No. 9003459) phases, so a higher temperature is necessary for the complete reaction and formation of the ternary $Sn_3Sb_2S_6$ phase.

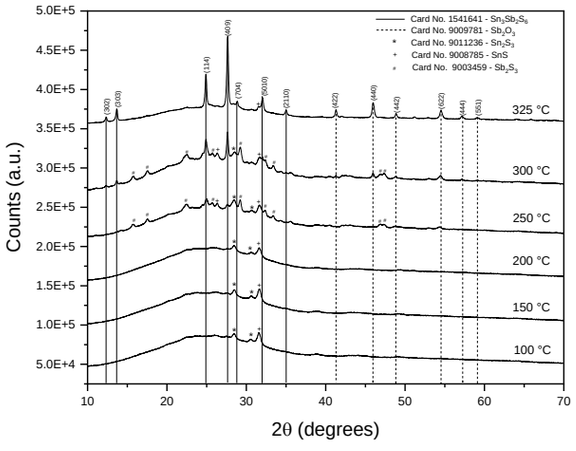


**Graphic 1** XRD diffractograms of glass/SnS/$Sb_2S_3$ multilayers heated at 100 °C, 150 °C, 200 °C, 250 °C, 300 °C and 325 °C in air.

At a temperature of 300 °C, additional peaks of $Sn_3Sb_2S_6$ phase appear at 2θ = 12.36°, 13.68°, 31.99° and 34.98°, corresponding to the planes (3 0 2), (3 0 3), (5 0 10) and (2 1 10), respectively. Moreover, the intensity of the (1 1 4) and (4 0 9) increases, indicating an improvement of crystallization. In addition, it is evident the formation of $Sb_2O_3$ phase (Card. No. 9009781), this is due to the exposure of $Sb_2S_3$ with $O_2$ during heating.

Finally, at a temperature of 325 °C, peaks of $Sn_3Sb_2S_6$ phase increases in intensity, the intensity of these peaks is higher compared to the peaks of $Sb_2O_3$ phase, which indicates that $Sn_3Sb_2S_6$ is present as the major phase and $Sb_2O_3$ is the secondary one. No peaks of $Sb_2S_3$ and SnS phases are present at 325 °C, indicating that the reaction of the precursor layers is over and no more $Sn_3Sb_2S_6$ can be formed.

Crystal size of the thin films was calculated using the highest intensity peak by using the Scherrer´s formula given by:

$$D = \frac{0.9\lambda}{\beta cos\theta} \quad (1)$$

Where λ is the wavelength of the incident X-ray radiation (1.5406 Å), β is the full width at half maximum of the diffraction peak at 2θ, and D is the crystallite size (A. Harizi, 2016). The crystallite size were 20.8 nm, 35.5 nm, and 38.6 nm, for the multilayers heated at 250 °C, 300 °C, and 325 °C, respectively. The crystallite size increases as the temperature increases due to the sintering process, that is a thermally activated process in which diffusion of species from high concentration region to low concentration region takes place, and big grains grow at expense of small grains.

To determine the preferential orientation, the texture coefficient was calculated form the reflection planes by using the following formula (Mindong Zheng, 2016):

$$TC_{(hkl)} = \frac{I_{(hkl)} \Big/ I_{o(hkl)}}{\frac{1}{N}\sum_{N=1}^{N} I_{(hkl)} \Big/ I_{o(hkl)}} \quad (2)$$

Where $I_{(hkl)}$ and $I_{o(hkl)}$ are the measured and standard intensities, respectively, and N es the number of available diffraction peaks from the diffractogram. The preferred orientation for the samples heated at 250 °C, 300 °C and 325 °C were the planes (1 1 4), (5 0 10), and (5 0 10), respectively.

Graphic 2 shows the optical characteristics of the samples heated at 100 °C, 250 °C, 300 °C, and 325 °C. From the % transmittance and % reflectance measurements, the absorption coefficient was calculated using the following formula (J.O. Gonzalez, 2014):

ISSN 2523-6873

$$\alpha = \frac{1}{d} In \left[ \frac{(1 - \%R)^2}{\%T} \right] \quad (3)$$

Where α is the absorption coefficient measured in $cm^{-1}$, d is the film thickness, in our experiments the measured thickness was ~ 1000 nm, %T is the percentage of transmittance and %R is the percentage of reflectance. In graphic 2 c) the absorption coefficients for the samples are shown, from the graphic is evident that all samples have high absorption coefficients ~ $10^5$ $cm^{-1}$ in the visible range, which means that small thickness is necessary to absorb most of the incident radiation.

From the spectra, the optical band gap of the samples was calculated using the formula, id.:

$$(\alpha h\nu)^{1/2} = A(h\nu - E_g) \quad (4)$$

Where $E_g$ is the optical band gap, the exponent of ½ indicates an allowed indirect transition, α is the absorption coefficient at a frequency *v*, and A is a constant. From graphic 2 d), all samples showed band gaps near 1 eV.

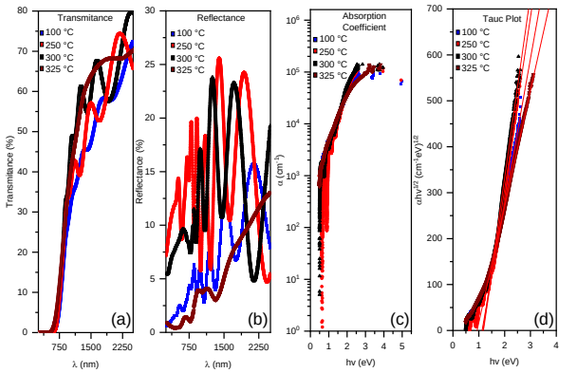


**Graphic 2** Optical characteristics of samples heated at 100 °C, 250 °C, 300 °C, and 325 °C in air. a) % Transmittance, b) % Reflectance, c) Absorption coefficient, and d) Tauc plot.

Graphic 3 shows the electrical characteristics of the samples heated at 100 °C, 250 °C, 300 °C, and 325 °C. In the graphic, both, photocurrent and IV curves of the samples are shown. The IV curve of the samples follows the ohm´s law, in which, current and voltage varies linearly; this is, as voltage increases current increases.

We observe that conductivity of sample heated at 100 °C is higher than conductivities of samples heated at 250°C and 300 °C, this may be due to the formation of $Sb_2S_3$ phase these temperatures, which is a highly resistive material (Sarah Messina, 2009). For the samples heated at 250°C, 300°C and 325 °C the photo response and conductivity increases, this may be due to the formation of $Sn_3Sb_2S_6$ phase, additionally, as the temperature increases conductivity increases due to the increase of grain size and crystallinity of the ternary compound.

As grain size increases, defects in the material, such as voids, grain boundaries, etc, that act as traps, reduces, decreasing the probability of recombination and the mobility of carries is improved as well as conductivity. The photo response of the samples was carried out by applying a bias voltage of 20 V and measure the current at dark and under illumination, 20 s at dark, 20 s under illumination and again 20 s at dark. When samples are illuminated, electrons from the valence band are promoted to the conduction band by absorbing photons with energy equal or greater than the band gap, current is increased due to more carriers are available for conduction. All samples show good photoconductivity behavior.

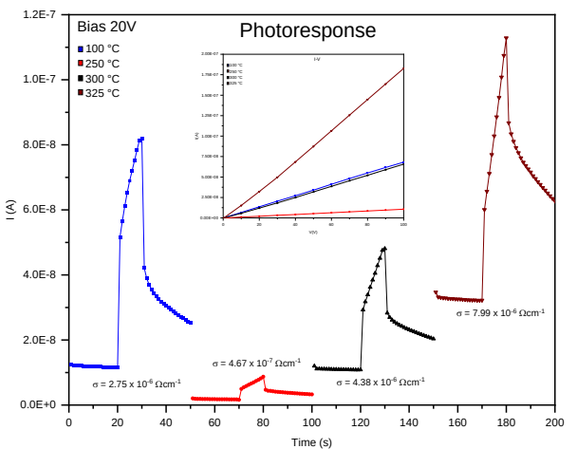


**Graphic 3** Electrical characteristics of samples heated at 100 °C, 250 °C, 300 °C, and 325 °C in air.

## 4. Acknowledgements

The authors are thankful to Conacyt – Fondo Sectorial de Investigación para la Educación for financial support. Authors are thankful to Dr. David Avellaneda from FIME-UANL for Uv-Vis-IR measurements.

ISSN 2523-6873

**5. Financing**

This work has been funded by CONACYT [grant number A1-S-46032, 2017-2018].

**6. Conclusions**

$Sn_3Sb_2S_6$ thin films were prepared by heating multilayers of glass/SnS/$Sb_2S_3$ at different temperatures in air. XRD studies indicate that $Sn_3Sb_2S_6$ begins formation at 250°C, and a temperature of 325°C it is completely formed. Texture coefficient showed a preferential orientation along the (1 1 4) plane for sample heated at 250 °C and (5 0 10) plane for samples heated at 300°C and 325 °C. Optical properties of the films showed high absorption coefficients in the order of $10^5$ $cm^{-1}$, and indirect allowed optical transitions with band gaps near 1 eV. The electrical properties of the samples were determined, samples showed conductivities in the order of $10^{-6}$ $\Omega cm^{-1}$, and an improvement in the electrical conductivity for $Sn_3Sb_2S_6$ thin films was observed as temperature increases.

**7. References**

A. Gassoumi, M. K. (2011). Growth and post-annealing effect on the properties of the new sulfosalt SnSb2S4 thin films. *Physica E*, 71-74. doi:https://doi.org/10.1016/j.physe.2011.07.007

A. Harizi, M. B. (2016). Substrate temperature dependence of structural, morphological and optical properties of Sn4Sb6S13 thin films deposited by vacuum thermal evaporation. *Materials Research Bulletin*, 52-62. doi:https://doi.org/10.1016/j.materresbull.2016.02.043

A. Larbi, H. D. (2014). Effect of substrate temperature on structural and optical properties of the new high absorbent Sn3Sb2S6 thin films. *Vacuum*, 34-39. doi:https://doi.org/10.1016/j.vacuum.2014.08.009

Aiswarya Nadukkandy, S. S.-M. (2023). Cubic structured silver antimony sulfide-selenide solid solution thin films for sustainable photodetection and photovoltaic application. *Journal of Alloys and Compounds*, 169072. doi:https://doi.org/10.1016/j.jallcom.2023.169072

Auttasit Tubtimtae, P. P. (2021). Indium dopant-induced morphological and optical properties of tin-antimony sulfide thin films synthesized by spin coating method compared with ab initio calculation. *Materials letters*, 130140. doi:https://doi.org/10.1016/j.matlet.2021.130140

D. Abdelkader, M. B. (2014). Investigation on optical properties of SnxSbySz sulfosalts thin films. *Materials Science in Semiconductor Processing*, 14-19. doi:https://doi.org/10.1016/j.mssp.2014.01.027

David Avellaneda, G. D. (2007). Structural and chemical trasnformations in SnS thin films used in chemically deposited photovoltaic cells. *Thin solid films*, 5771 - 5776. doi:https://doi.org/10.1016/j.tsf.2006.12.078

E.I. Emon, A. I. (2023). A comprehesive photovoltaic study on tungsten disulfide (WS2) buffer layer based CdTe solar cell. *Heliyon*, e14438. doi:https://doi.org/10.1016/j.heliyon.2023.e14438

J.O. Gonzalez, S. S. (2014). Photovoltaic structures using AgSb(SxSe1-x)2 thin films as absorber. *Applied Physics A*, 2095 - 2105. doi:10.1016/j.solmat.2012.04.008

Jiayou Xue, X. Y. (2023). Improved Carrier Lifetimes of CdSe Thin Film via Te Doping for Photovoltaic Application. *ACS Applied Materials & Interfaces, 15*(14), 17858–17866. doi:https://doi.org/10.1021/acsami.3c00461

Mindong Zheng, J. N.-C. (2016). Effect of annealing temperatur on the crystalline structure, growth behaviour and properties of SnO2:Sb thin films prepared by radio frequency (RF)-magnetron sputtering. *Journal of Alloys and Compounds*, 371-378. doi:https://doi.org/10.1016/j.jallcom.2015.12.037

N. Ali, R. A. (2015). A novel approach for the synthesis of tin antimony sulphide thin films for photovoltaic application. *Solar Energy*, 25-33. doi:https://doi.org/10.1016/j.solener.2014.12.021

ISSN 2523-6873

Nisar Ali, S. H. (2013a). Effect of air annealing on the band gap and optical properties of SnSb2S4 thin films for solar cell application. *Materials Letters*, 148-151. doi:https://doi.org/10.1016/j.matlet.2013.02.097

Nisar Ali, S. H. (2013b). Structural and optoelectronic properties of antimony tin sulphide thin films deposited by thermal evaporation techniques. *Optik*, 4746-4749. doi:https://doi.org/10.1016/j.ijleo.2013.01.086

Sarah Messina, M. N. (2009). Solar cells with Sb2S3 absorber films. *Thin Solid Films*, 2503-2503. doi:https://doi.org/10.1016/j.tsf.2008.11.060

Sebin Devasia, S. S. (2020). Tin antimony sulfide (Sn6Sb10S21) thin films by heating chemically deposited Sb2S3/SnS layers: Studies on the structure and their optoelectronic properties. *Journal of Alloys and Compounds*, 154256. doi:https://doi.org/10.1016/j.jallcom.2020.154256

Taoufik Chargui, F. L.-H. (2023). Experimental and numerical study of the CIGS/CdS heterojunction solar cell. *Optical Materials*, 113849. doi:https://doi.org/10.1016/j.optmat.2023.113849

ISSN 2523-6873

Article **Journal of Innovative Engineering**
June 2023 Vol.7 No.20 22-30

# Destructive Test in 3D Printing

# Ensayo Destructivo en Impresión 3D

LERMA-GARCÍA, Miguel Angel†*, ROSALES-GALLEGOS, Israel Atzin, TUDÓN-MARTÍNEZ, Alberto and DOMÍNGUEZ-HERNÁNDEZ, Carlos Alberto

*Universidad Tecnológica de San Luis Potosí, Prol. Av. Dr. Arturo Nava Jaimes, Rancho Nuevo, Soledad de Graciano Sánchez, S. L. P.*

ID 1st Author: *Miguel Angel, Lerma-García* / **ORC ID:** 0000-0002-7849-4528, **Researcher ID Thomson:** IWE-1628-2023**, CVU CONAHCYT ID:** 668648

ID 1st Co-author: *Israel Atzin, Rosales-Gallegos* / **ORC ID:** 0000-0003-1485-9601, **Researcher ID Thomson:** AAR-7809-2021, **CVU CONAHCYT ID: 372002**

ID 2nd Co-author: *Alberto, Tudón-Martínez* / **ORC ID:** 0000-0003-1689-1250, **CVU CONAHCYT ID:** 411753

ID 3rd Co-author: *Carlos Alberto, Domínguez-Hernández* / **ORC ID:** 0000-0002-4628-0883, **CVU CONAHCYT ID:** 1204882

**DOI**: 10.35429/JOIE.2022.20.7.22.30 Received March 16, 2023; Accepted June 30, 2023

**Abstract**

Today it is essential for any manufacturing company, to be able to have information about the effectiveness of the designs, as well as the quality of its raw materials, due to this, one of the key strategies is the prototyping of parts through additive manufacturing, the objective of this article is to provide information about the structural resistance of a 3D printed component through the effectiveness in the deposition of extruded filament and according to a deposition made, the implicit variables for both cases will be determined, which will be measured by tests. destructive, identifying values of deformation versus effort and will contribute to the determination of advantages and disadvantages of the impression, as well as the position with which the deposition is made.

**Printing, Resistance, Test**

**Resumen**

Hoy en día es imprescindible para cualquier empresa manufacturera, el poder tener información acerca de la efectividad de los diseños, así como de la calidad de sus materias primas, debido a ello una de las estrategias clave es el prototipado de partes mediante manufactura aditiva, el objetivo de este artículo es proveer información acerca de la resistencia estructural de un componente impreso en 3D mediante la efectividad en la deposición de filamento extruido y de acuerdo a una deposición efectuada, se determinarán las variables implícitas para ambos casos, las cuáles se medirán mediante ensayos destructivos, identificando valores de deformación versus esfuerzo y se contribuirá en la determinación de ventajas y desventajas de la impresión, así como la posición con la se realiza la deposición.

**Impresión, Resistencia, Ensayo**

**Citation:** LERMA-GARCÍA, Miguel Angel, ROSALES-GALLEGOS, Israel Atzin, TUDÓN-MARTÍNEZ, Alberto and DOMÍNGUEZ-HERNÁNDEZ, Carlos Alberto. Destructive Test in 3D Printing. Journal of Innovative Engineering. 2023. 7-20: 22-30

*Correspondence to Author (e-mail: mlerma@utslp.edu.mx)
† Researcher contributing as first Author.

 

## Introduction

3D printing is an additive manufacturing method, with which prototype models or functional work components can be generated, this method involves the application of material input, which can be of different properties and characteristics, among the most used:

– PLA
– ABS
– Resin
– Metallic powders.

This technique is very useful for the production of parts, however, in the manufacturing process that ranges from design to preparation, it is vitally important to identify the best position of the component, which will structurally define the way in which which the filler material will be deposited and in the definition of the Cartesian trajectories in which the printing machine generates the material deposition.

In addition to the above, the way in which the position of the element to be printed is defined will depend on its geometry, since from this it will depend on the need for support, the printing time, the amount of material input and the structural resistance of the component, due to this, the present investigation will identify these change factors and through a destructive stress test, the effectiveness of the method in relation to the direction of material deposition can be measured.

The relationship of the deformation factor (dependent variable) with respect to the stress factor (independent variable) and through a plastic specimen with PLA material in a configuration directed from the design process, preparation of files according to the extension of the modeling software , preparation process for post-processing, execution of 3D printing in horizontal and vertical position and application of tests, will allow observing the result of the implicit variables in each proposal and verified by applying destructive testing.

## Development of Sections and Sections of the Article with subsequent numbering

In the application of the destructive test to identify the resistance in the proposed specimens, it is important to work in the following stages, which are:

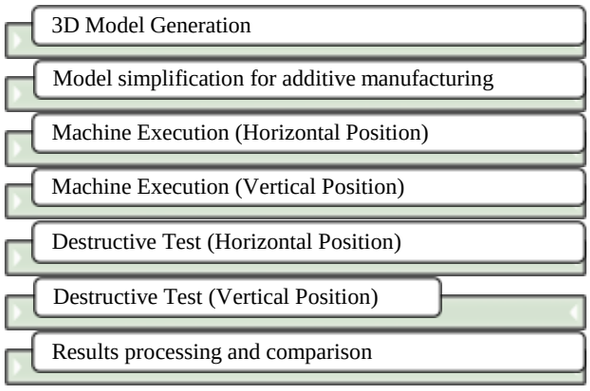


**Figure 1** Stages of 3D printing and destructive testing (Boisas, 2018)

### 1. Design of the 3D model

The design of the 3D model, part of the GeDG (Computer extended Descriptive Geometry) structure, which is oriented to a sequence of geometric construction, this leads the generation of the model to focus on dimensional qualities in a graphical environment, which provides Cartesian positions in the generation of the element, of which axes x, y and z.

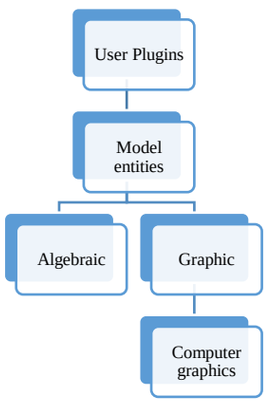


**Figure 2** Modelo GeDG
*(Prado-Velasco, García-Ruesgas, Ortíz-Martín 2023)*

Taking the previous structure as a reference, the specimen is modeled in the CAD software environment and under the standard (ASTM D638), the three-dimensional design is generated according to the resistance of the material to be used (PLA).

ISSN 2523-6873

For the beginning of the design of the specimen, a round smooth head specimen is considered, with origin in Cartesian coordinates at 0.

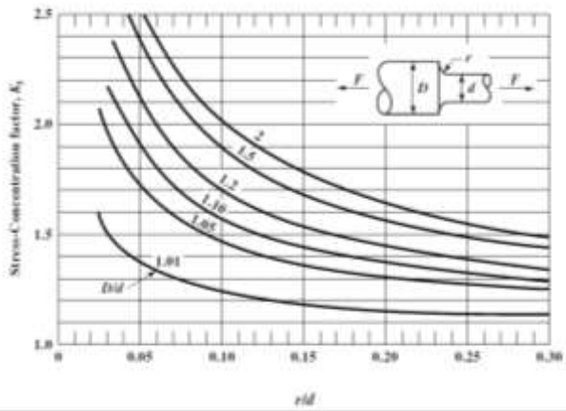

**Figure 3** Factor stress-concentration
*(McCauley, 2013)*

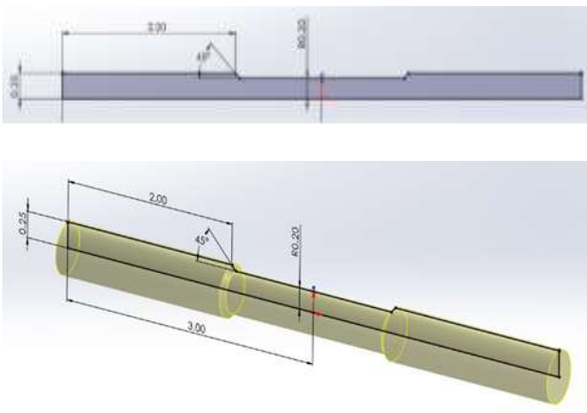

**Figure 4** Zero Origin Specimen Design
*(Contribution to the project, unpublished)*

## 2. Simplification of the model for additive manufacturing

The three-dimensional model is a very important factor in the preparation process for printing, since according to the GeDG structure approach, it supposes a solid element, since in the software environment the element is floating, it must be to achieve a preparation of the modeling, this by means of a recognition of nodes from a binary element.

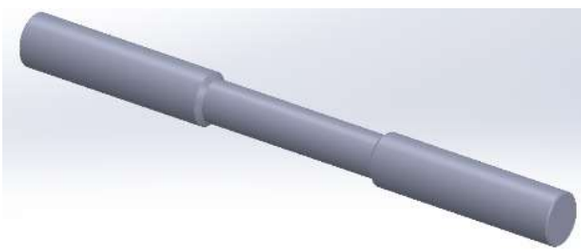

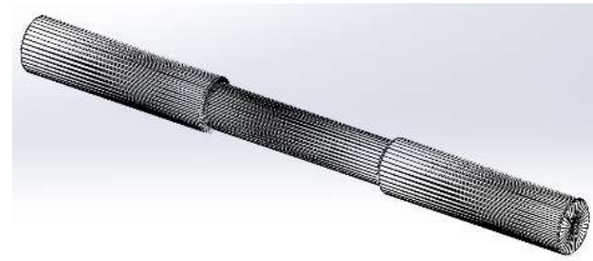

**Figure 5** Design simplification
*Contribution to the project, unpublished*

During the model simplification process, each binary element of the model is configured to the origin in the Cartesian system, which generates a position value in space. Said value will be determined from the import of the file in post software. processed for geometric recognition, and trajectory assignment.

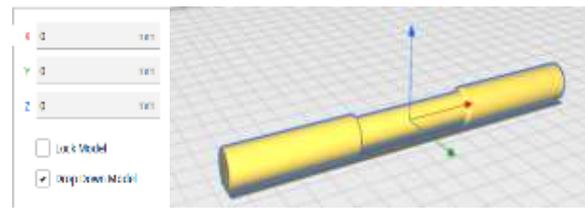

**Figure 6** Geometric Recognition, horizontal position (Contribution to the project, unpublished)

After the geometric recognition stage, the positions of each binary element of the component will be identified and a translation process into standard language, better known as G Language, will be generated through which the printing process can be governed, through a sequence of codes and trajectories in a Cartesian plane with which the deposition of material will be achieved at each necessary space and corresponding to the model in three dimensions and supported with a 3D printing machine with a base extruder at temperature conditions between 180 and 200 ° c.

ISSN 2523-6873

| | |
|---|---|
| ;FLAVOR:Marlin<br>;TIME:1763<br>;Filament used: 3.89792m<br>;Layer height: 0.3<br>;MINX:117.489<br>;MINY:190.45<br>;MINZ:0.3<br>;MAXX:282.508<br>;MAXY:209.897<br>;MAXZ:12.6<br>;Generated with Cura_SteamEngine 5.2.2<br>M140 S60<br>M105<br>M190 S60<br>M104 S200<br>M105<br>M109 S200<br>M82 ;absolute extrusion mode<br>M107 ;Start with the fan off | G92 E0<br>G92 E0<br>G1 F2400 E-6<br>;LAYER_COUNT:42<br>;LAYER:0<br>M106 S255<br>M204 S3000<br>M205 X10 Y10<br>G1 F600 Z0.375<br>G0 F3000 X120.935 Y191.511 Z0.375<br>M204 S1800<br>M205 X8 Y8<br>;TYPE:SKIRT<br>G1 F600 Z0.3<br>G1 F2400 E0<br>G1 X121.571 Y191.183 E0.04998<br>G1 X122.239 Y190.929 E0.0999<br>G1 X122.932 Y190.751 E0.14987<br>G1 X123.761 Y190.634 E0.20835 |

**Table 1** Horizontal ISO language (Project contribution, unpublished)

## 3. Machine Execution (Horizontal Position)

During the machine execution process, there is a simulation stage, which will show the user the trajectories defined according to the binary system, which is translated into ISO language by post-processing software algorithms. It is important to mention that the Characteristics can be of a proposed nature or can be customized by the user according to the geometric characteristics.

According to Güler Özgül, H.., & Tatlı, O. (2021), considering these factors is a highly relevant issue since the difference between geometries, as well as the direction during the deposition of material, may have different mechanical properties, which will contribute to the different resistance values depending consequently on the location and load that acts on them when constituting a geometric structure

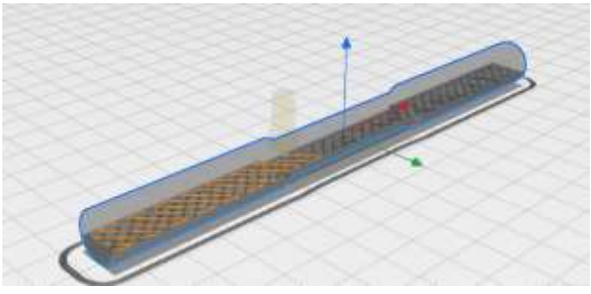

**Figure 7** Preview horizontal trajectories, (Contribution to the project, unpublished)

Once it has been identified by the user that the trajectories have been recorded, it is transferred to a removable memory, in which the standard programming language (Language G) will be stored and it will be physically connected to the printing machine to start with the manufacturing process by additive manufacturing (3D printing).

The 3D printing machine must cover work parameters in order to carry out the deposition efficiently, among which:

– Extrusion temperature (200°C)
– Printing table temperature (60°C)

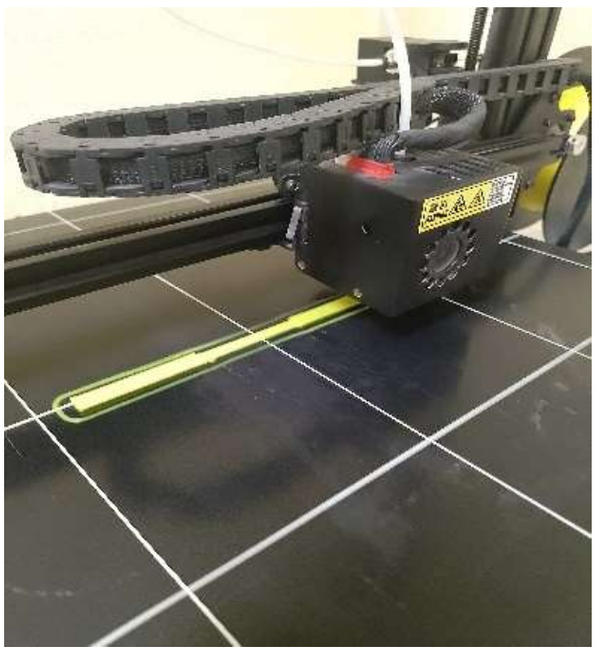

**Figure 8** Landscape 3D printing
*(Contribution to the project, unpublished)*

## 4. Machine Execution (Vertical Position)

After the horizontal prints, the prints will be made in a vertical position, it should be noted that the machine parameters are the same, which were described in the previous section and the change factor for printing these tests will be the position In this process, once both samples are finished, the resistance given according to the material deposition will be identified.

It is important to highlight that during the parameter setting process, the capacity dimensions of the printer must be considered, according to its total height, since a maximum degree of opening must be avoided, at the same time that it must be avoid collision during the deposition process.

ISSN 2523-6873

Of the extruder with respect to the test tube, since its base area is proportional to the dimension of the standardized test tube, which generates a possible detachment of the printing table at the moment of being displacing the extruder on the axes considered during the post-processing process when generating the ISO printing program.

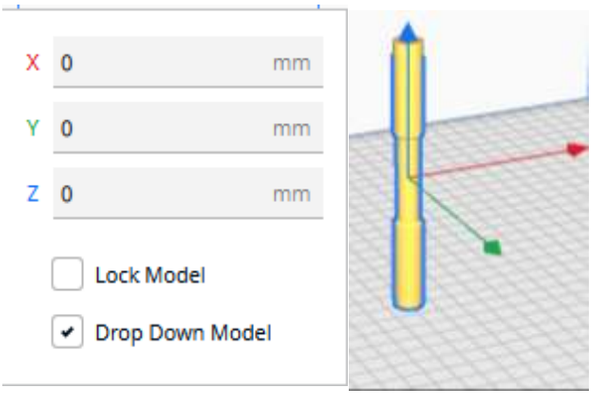


**Figure 9** Geometric recognition, vertical position,
*(Contribution to the project, unpublished)*

| | |
|---|---|
| ;FLAVOR:Marlin<br>;TIME:2739<br>;Filament used: 3.80996m<br>;Layer height: 0.3<br>;MINX:186.955<br>;MINY:186.953<br>;MINZ:0.3<br>;MAXX:213.044<br>;MAXY:213.036<br>;MAXZ:152.4<br>;Generated with Cura_SteamEngine 5.2.2<br>M140 S60<br>M105<br>M190 S60<br>M104 S200<br>M105<br>M109 S200<br>M82 ;absolute extrusion mode<br>M107 ;Start with the fan off | G92 E0<br>G1 F2400 E-6<br>;LAYER_COUNT:508<br>;LAYER:0<br>M106 S255<br>M204 S3000<br>M205 X10 Y10<br>G1 F600 Z0.375<br>G0 F3000 X190.606 Y190.949 Z0.375<br>M204 S1800<br>M205 X8 Y8<br>;TYPE:SKIRT<br>G1 F600 Z0.3<br>G1 F2400 E0<br>G1 X191.327 Y190.257 E0.0698<br>G1 X192.184 Y189.548 E0.14749<br>G1 X193.1 Y188.93 E0.22467<br>G1 X194.042 Y188.39 E0.30051<br>G1 X195.001 Y187.952 E0.37414<br>G1 X195.514 Y187.758 E0.41245 |

**Table 2** Vertical ISO language
*(Project contribution, unpublished)*

In the sequence of machine execution stage 4, of the printing process in vertical position, the post-processing software adjusts to a different sequence of the trajectory in the coordinate system, said process performs the simulation of plastic deposition PLA.

In which a different process is observed in the application of the material, but the same in the geometric shape of the standardized specimen.

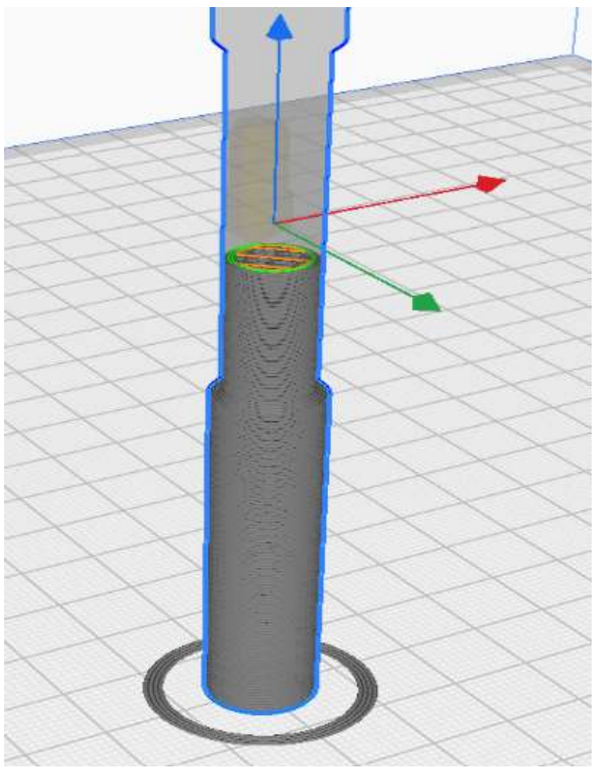

**Figure 10** Preview vertical paths
*(Contribution to the project, unpublished)*

Once the trajectories have been simulated by the software and no interferences have been detected in the code, the standard programming language (Language G) is once again transferred to carry out the manufacturing process by additive manufacturing (3D printing), this time in a vertical position.

The work parameters must be reviewed again in order to carry out the deposition efficiently, the following will be considered again:

– Extrusion temperature (200°C)
– Printing table temperature (60°C)

ISSN 2523-6873

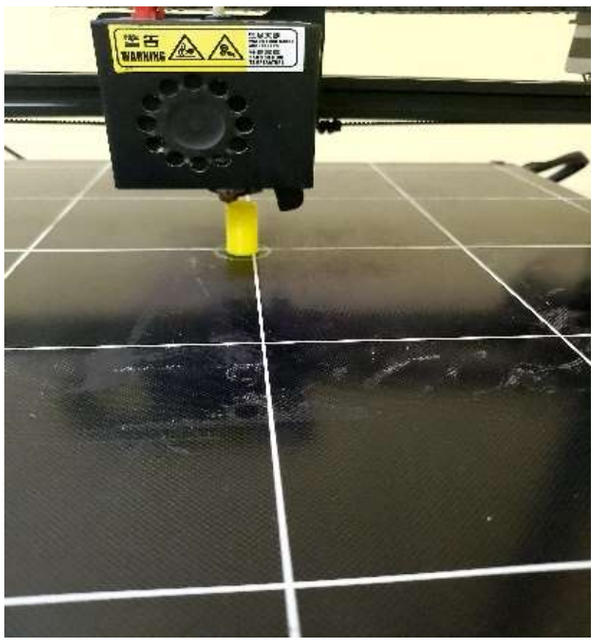

**Figure 11** Vertical 3D printing
*(Contribution to the project, unpublished)*

## 5. Destructive Test (Horizontal position)

By definition, a destructive test is the verification of mechanical properties, which can be:

– Static: Hardness, traction, compression, shearing, bending, buckling, creep.

– Dynamic: Shock resistance, wear, fatigue (Moreno, López-González, Malagón-Mendoza, Henao-Vega, 2006).

For the present investigation, a tension study will be applied, this concept is based on a physical study in which a solid is subjected to the action of a system of external forces, which is recognized when there is the application of loads and consequently a reaction is obtained, which is why it is defined that any member that supports a load is deformed by the influence of the applied load according to its direction and magnitude, which will be proportional and transversal to its section area (Mott, R. L. , Salas, R.N., Flores, M.A.R., & Martínez, E.B.-2009).

The direct action of the application of loads in a solid is represented by the presence of forces in interaction through the surface, these forces achieve an interaction, they are equal in opposite directions on the contact sections (Cervera-Ruiz, Blanco-Díaz, 2002).

The relationship in this interaction process is achieved in the proportion in which the force or load acting on a surface generates a condition called effort, which is denoted by the assignment of the Greek letter sigma σ.

According to the direction in which the force is applied, two types of effort are obtained, of which:

– Compression stress, which occurs to the extent that the action of the forces is collinear, that is, in the same direction.

– Effort of tension or traction, which occurs to the extent that the action of the forces is concurrent, ie in the opposite direction.

Once the relationship to the cross-sectional area has been identified, it will be possible to identify the effects of effort and force (Guzmán, 2005).

$$\sigma = \frac{F}{A} \tag{1}$$

According to the previous theorem, a test will be considered taking into account the action of the force applied in a uniaxial manner and a section of cross-sectional area of the specimen that was printed horizontally, this to identify the effort to which it is subjected. and identify the value of the maximum force and the resulting deformation, this process will be carried out in a WAW-1000D destructive testing equipment, this machine allows the specimen to be held according to its geometry, which can be flat or with a cylindrical head,

For the present study, a change in the clamping means is considered through the jaws, since the geometry is cylindrical, for which smooth head jaws will be used, with a V-cut, which is determined to achieve effectiveness. in the process of measuring the resistance of the component, which according to the shape and dimensions of the test tube for each case, will consider the uniform cross section and its type of manufacturing process, which may include cast test tubes and test tubes with or without machining, which will be essential in the study to obtain the necessary measurement data and according to the variables that are sought to be obtained from the study CASTRILLÓN, A. A., & TORRES, M. R. M. (2017).

ISSN 2523-6873


**Figure 12** Destructive test, horizontal specimen
*(Contribution to the project, unpublished)*

For the validation of the destructive test, a population sample size of 50 test tubes is being considered, of which the following will be measured:

– Upper Yield Force
– Stress
– Deformation

Likewise, the Average value of the sample and the limits of the test will be validated, this as a method of consideration of the consistency of the test and biases in the study.

| 3D printed specimens in horizontal position | | | | |
|---|---|---|---|---|
| No. Test | UYF (N) | Strees (Pa) | Deformation | Test speed |
| 1 | 81 | 1031452 | 0.0003126 | 5 N/S |
| 2 | 78 | 993250 | 0.0003010 | |
| 3 | 77 | 980517 | 0.0002971 | |
| 4 | 78 | 993250 | 0.0003010 | |
| 5 | 72 | 916847 | 0.0002778 | |
| 6 | 79 | 1005984 | 0.0003048 | |
| 7 | 73 | 929581 | 0.0002817 | |
| 8 | 73 | 929581 | 0.0002817 | |
| 9 | 80 | 1018718 | 0.0003087 | |
| 10 | 73 | 929581 | 0.0002817 | |

**Table 3** Measurement of Upper Yield Force, Horizontal Specimen (UYF)
*(Contribution to the project, unpublished)*

During data processing and considering the relationship between tests, it is observed that the individuals in the population have a normal discrepancy among themselves, but they remain at control values, which translates into a correct application of the test.

– MEAN: 75.64 N
– UCL: 87.42 N
– LCL: 63.86 N

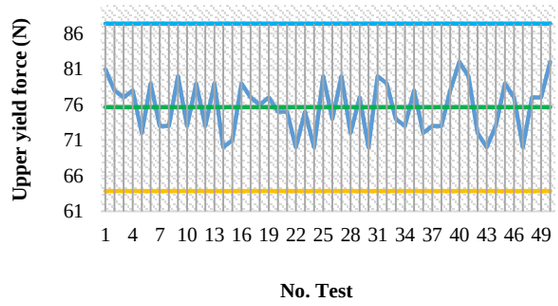


**Graphic 1** Control Chart UYF horizontal
*(Contribution to the project, unpublished)*

In the process of application of the load during the test, it can be seen that the rupture condition occurs at an average value of 75.64N, at this stage a detachment of filaments can be seen, which manage to behave as tensioned threads at a maximum load, to later generate a detachment by uniaxial action, by determination it is appreciated that fatigue is directly related to the degree of resistance that the presence of filaments opposes in the construction architecture, which according to Becerra, J. L., Díaz-Rodríguez , J. G., & González-Estrada, O. A. (2020), is obtained using a concentric and isotropic arrangement of fiber reinforcement, which interlocks the deposition groups parallel to the section set.

**Figure 13** Destructive test horizontal position
*(Contribution to the project, unpublished)*

Due to the type of test and the 3d printing position in the manufacturing process of the specimen, an elongation is observed, which manages to be translated and calculated by means of the value of the deformation which is present in the given value of the effort and the elastic modulus (Guzmán, 2005).

$$\varepsilon = \frac{\sigma}{E} \quad (2)$$

ISSN 2523-6873

## 6. Destructive Test (Vertical Position)

In this stage of the test, the condition in the manufacture of the test tube is changed, which, as explained in stage 4, will be carried out by deposition of PLA material in a position parallel to the extrusion axis and in a vertical direction to the printing table. , which under the same criteria in the WAW-1000D machine, will be measured:

– Upper Yield Force
– Stress
– Deformation

| 3D printed specimens in vertical position | | | | |
|---|---|---|---|---|
| No. TEST | UYF (N) | Strees (Pa) | Deformation | Test speed |
| 1 | 55 | 700369 | 0.0002122 | 5 N/S |
| 2 | 54 | 687635 | 0.0002084 | |
| 3 | 59 | 751305 | 0.0002277 | |
| 4 | 56 | 713103 | 0.0002161 | |
| 5 | 50 | 636699 | 0.0001929 | |
| 6 | 58 | 738571 | 0.0002238 | |
| 7 | 59 | 751305 | 0.0002277 | |
| 8 | 65 | 827709 | 0.0002508 | |
| 9 | 56 | 713103 | 0.0002161 | |
| 10 | 52 | 662167 | 0.0002007 | |

**Table 4** Measurement of Upper Yield Force, vertical specimen (UYF) (Contribution to the project, unpublished)

During the test, a normal discrepancy is observed, which translates into a correct application of the same, which translates into the following values:

– MEAN: 57.24 N
– UCL: 70.48 N
– LCL: 44 N

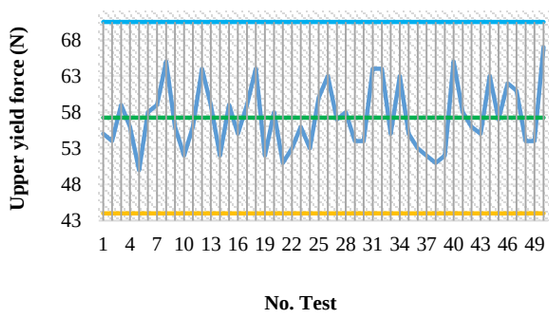


**Graphic 2** Control Chart UYF vertical
*(Contribution to the project, unpublished)*

In the test application, it can be observed that the rupture condition occurs at an average value of 57.24N and consequently the elongation characteristics are not present, instead a detachment of section between filaments is observed, which are arranged in a circular way resembling a set of necklaces

**Figure 14** Destructive test vertical position (Contribution to the project, unpublished)

## 7. Data processing and results

The data comparison reflects a difference focused on the application of force and structural rupture, in which a greater application of this is observed in the 3D printing samples in a horizontal position, compared to the 3D printing samples in a vertical position.

| 3D print horizontal | 3D print vertical |
|---|---|
| MEAN: 75.64 N | MEAN: 57.24 N |
| UCL: 87.42 N | UCL: 70.48 N |
| LCL: 63.86 N | LCL: 44 N |

**Table 5** Comparison of UYF, UCL and LCL data
*(Contribution to the project, unpublished)*

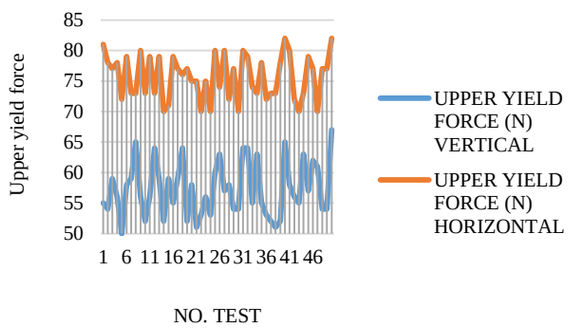


**Graphic 3** Comparison
*(Contribution to the project, unpublished)*

## Financing

This research work and application of tests has been financed by the UTSLP (Technological University of San Luis Potosí), as a means of research development and content publication, which is contemplated in the Institutional POA (SA7 Program K09.03_010103 " Publication of articles and attendance at congresses)

ISSN 2523-6873

## Conclusions

The application of destructive tests to a 3D printed element is of vital importance, since through the results of the tests, the best position is determined during the material deposition process, as is the case of the present study, since it can Verify that according to the geometry of the printed body and its position through extrusion, it will determine the tensile strength, this according to the results obtained in the proposed tests, it is concluded that the direction of the filaments of the material of The contribution is significant to the presence of uniaxial yield forces, as long as their direction coincides with that of the extruded filaments.

A recommendation aimed at improving this test measurement process is to check the elastic modulus of the material to be studied, which is significant due to its intrinsic properties and according to its nature, composition and mechanical properties, since these will determine directly the result obtained from the calculations at the time of carrying out the test, likewise it must be considered that the type of material to be printed, as well as the variables to be evaluated, will be according to their properties and depending on the parameterization machine (3D printer) during the material deposition process.

In addition, it is highlighted that, under the action of fluctuating stresses, in this case it consequently generates fatigue, which is evident through visual effects and transversely measurable at the moment of applying the load, which is continuous and constant in unit value, generating a structural phenomenon called "fatigue", which as a result leads to the collapse of the specimen (fracture) SUÁREZ, H. E. J. (2017).

## References

Boisas, G. M. (2018). Introducción a la Fabricación Aditiva, (Cómo y Porqué de la Impresión3D). http://hdl.handle.net/11531/70587

Becerra, J. L., Díaz-Rodríguez, J. G., & González-Estrada, O. A. (2020). Daño en partes de manufactura aditiva reforzadas por fibras continuas. Revista UIS ingenierías, 19(2), 161-176. https://doi.org/10.18273/revuin.v19n2-2020018

CASTRILLÓN, A. A., & TORRES, M. R. M. (2017). Ensayos de tensión (I). Pontificia Universidad Javeriana. https://doi.org/10.2307/j.ctv19qmdpw

Guzman, J. M. C. (2005). Ensayos Destructivos Y No Destructivos De Probetas De Acero Soldadas Con Electrodos Revestidos.

Güler Özgül, H. ., & Tatlı, O. . (2021). Mechanical characterization of polylactic acid polymer 3D printed materials: the effects of infill geometry. Revista De Metalurgia, 57(3), e202. https://doi.org/10.3989/revmetalm.202

Prado-Velasco, M., García-Ruesgas, L., Ortíz-Marín, R., & Vázquez-López, E. (2023). Modelado paramétrico computacional de sistemas 3D mediante Geometría Descriptiva (CeDG): sistema diédrico. Aula Magna. https://doi.org/10.20944/preprints202303.0545.v1

McCauley, J. W., Strassburger, E., Patel, P., Paliwal, B., & Ramesh, K. T. (2013). Experimental observations on dynamic response of selected transparent armor materials. Experimental Mechanics, 53, 3-29. https://doi.org/10.1007/s11340-012-9658-5

Moreno, G., López, J., Malagón, O., & Henao, J. (2006). Diseño y construcción de una máquina básica de ensayos destructivos de tracción y torsión. Bogota, Colombia.

Mott, R. L., Salas, R. N., Flores, M. A. R., & Martínez, E. B. (2009). Resistencia de materiales (Vol. 5). Pearson Educación.

SUÁREZ, H. E. J. (2017). Resistencia de materiales. Algunos temas especiales (1st ed.). Programa Editorial Universidad Autónoma de Occidente. https://doi.org/10.2307/j.ctvckq88m

ISSN 2523-6873

# [Title in Times New Roman and Bold No. 14 in English and Spanish]

Surname (IN UPPERCASE), Name 1st Author†*, Surname (IN UPPERCASE), Name 1st Coauthor, Surname (IN UPPERCASE), Name 2nd Coauthor and Surname (IN UPPERCASE), Name 3rd Coauthor

*Institutional Affiliation of Author including Dependency (No.10 Times New Roman and Italic)*

*International Identification of Science - Technology and Innovation*

ID 1st Author: (ORC ID - Researcher ID Thomson, arXiv Author ID - PubMed Author ID - Open ID) and CVU 1st author: (Scholar-PNPC or SNI-CONAHCYT) (No.10 Times New Roman)

ID 1st Coauthor: (ORC ID - Researcher ID Thomson, arXiv Author ID - PubMed Author ID - Open ID) and CVU 1st coauthor: (Scholar or SNI) (No.10 Times New Roman)

ID 2nd Coauthor: (ORC ID - Researcher ID Thomson, arXiv Author ID - PubMed Author ID - Open ID) and CVU 2nd coauthor: (Scholar or SNI) (No.10 Times New Roman)

ID 3rd Coauthor: (ORC ID - Researcher ID Thomson, arXiv Author ID - PubMed Author ID - Open ID) and CVU 3rd coauthor: (Scholar or SNI) (No.10 Times New Roman)

(Report Submission Date: Month, Day, and Year); Accepted (Insert date of Acceptance: Use Only ECORFAN)

**Abstract (In English, 150-200 words)**

Objectives
Methodology
Contribution

**Keywords (In English)**

Indicate 3 keywords in Times New Roman and Bold No. 10

**Abstract (In Spanish, 150-200 words)**

Objectives
Methodology
Contribution

**Keywords (In Spanish)**

Indicate 3 keywords in Times New Roman and Bold No. 10

**Citation:** Surname (IN UPPERCASE), Name 1st Author, Surname (IN UPPERCASE), Name 1st Coauthor, Surname (IN UPPERCASE), Name 2nd Coauthor and Surname (IN UPPERCASE), Name 3rd Coauthor. Paper Title. Journal of Innovative Engineering. Year 1-1: 1-11 [Times New Roman No.10]

* Correspondence to Author (example@example.org)
† Researcher contributing as first author.

 

## Introduction

Text in Times New Roman No.12, single space.

General explanation of the subject and explain why it is important.

What is your added value with respect to other techniques?

Clearly focus each of its features

Clearly explain the problem to be solved and the central hypothesis.

Explanation of sections Article.

## Development of headings and subheadings of the article with subsequent numbers

[Title No.12 in Times New Roman, single spaced and bold]

Products in development No.12 Times New Roman, single spaced.

## Including graphs, figures and tables-Editable

In the article content any graphic, table and figure should be editable formats that can change size, type and number of letter, for the purposes of edition, these must be high quality, not pixelated and should be noticeable even reducing image scale.

[Indicating the title at the bottom with No.10 and Times New Roman Bold]

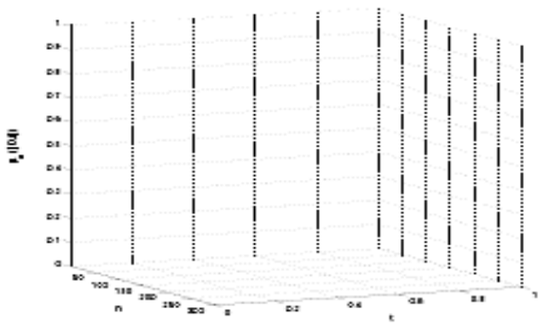

**Graphic 1** Title and *Source (in italics)*

Should not be images-everything must be editable.

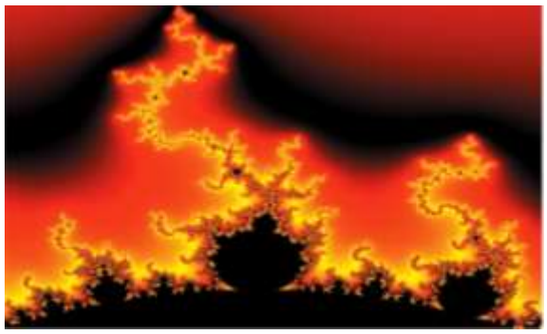

**Figure 1** Title and *Source (in italics)*

Should not be images-everything must be editable.

| | | | | |
|---|---|---|---|---|
| | | | | |
| | | | | |
| | | | | |
| | | | | |

**Table 1** Title and *Source (in italics)*

Should not be images-everything must be editable.

Each article shall present separately in **3 folders**: a) Figures, b) Charts and c) Tables in .JPG format, indicating the number and sequential Bold Title.

**For the use of equations, noted as follows:**

$$Y_{ij} = \alpha + \sum_{h=1}^{r} \beta_h X_{hij} + u_j + e_{ij} \qquad (1)$$

Must be editable and number aligned on the right side.

## Methodology

Develop give the meaning of the variables in linear writing and important is the comparison of the used criteria.

## Results

The results shall be by section of the article.

## Annexes

Tables and adequate sources

## Thanks

Indicate if they were financed by any institution, University or company.

ISSN 2523-6873

**Conclusions**

Explain clearly the results and possibilities of improvement.

**References**

Use APA system. Should not be numbered, nor with bullets, however if necessary numbering will be because reference or mention is made somewhere in the Article.

Use Roman Alphabet, all references you have used must be in the Roman Alphabet, even if you have quoted an Article, book in any of the official languages of the United Nations (English, French, German, Chinese, Russian, Portuguese, Italian, Spanish, Arabic), you must write the reference in Roman script and not in any of the official languages.

**Technical Specifications**

Each article must submit your dates into a Word document (.docx):

Journal Name
Article title
Abstract
Keywords
Article sections, for example:

*1. Introduction*
*2. Description of the method*
*3. Analysis from the regression demand curve*
*4. Results*
*5. Thanks*
*6. Conclusions*
*7. References*

Author Name (s)
Email Correspondence to Author
References

**Intellectual Property Requirements for editing:**

- Authentic Signature in Color of Originality Format Author and Coauthors
- Authentic Signature in Color of the Acceptance Format of Author and Coauthors
- Authentic Signature in Color of the Conflict of Interest Format of Author and Co-authors.

ISSN 2523-6873

**Reservation to Editorial Policy**

Journal of Innovative Engineering reserves the right to make editorial changes required to adapt the Articles to the Editorial Policy of the Research Journal. Once the Article is accepted in its final version, the Research Journal will send the author the proofs for review. ECORFAN® will only accept the correction of errata and errors or omissions arising from the editing process of the Research Journal, reserving in full the copyrights and content dissemination. No deletions, substitutions or additions that alter the formation of the Article will be accepted.

**Code of Ethics - Good Practices and Declaration of Solution to Editorial Conflicts**

**Declaration of Originality and unpublished character of the Article, of Authors, on the obtaining of data and interpretation of results, Acknowledgments, Conflict of interests, Assignment of rights and Distribution**

The ECORFAN-Mexico, S.C Management claims to Authors of Articles that its content must be original, unpublished and of Scientific, Technological and Innovation content to be submitted for evaluation.

The Authors signing the Article must be the same that have contributed to its conception, realization and development, as well as obtaining the data, interpreting the results, drafting and reviewing it. The Corresponding Author of the proposed Article will request the form that follows.

Article title:

- The sending of an Article to Journal of Innovative Engineering emanates the commitment of the author not to submit it simultaneously to the consideration of other series publications for it must complement the Format of Originality for its Article, unless it is rejected by the Arbitration Committee, it may be withdrawn.

- None of the data presented in this article has been plagiarized or invented. The original data are clearly distinguished from those already published. And it is known of the test in PLAGSCAN if a level of plagiarism is detected Positive will not proceed to arbitrate.

- References are cited on which the information contained in the Article is based, as well as theories and data from other previously published Articles.

- The authors sign the Format of Authorization for their Article to be disseminated by means that ECORFAN-Mexico, S.C. In its Holding Republic of Peru considers pertinent for disclosure and diffusion of its Article its Rights of Work.

- Consent has been obtained from those who have contributed unpublished data obtained through verbal or written communication, and such communication and Authorship are adequately identified.

- The Author and Co-Authors who sign this work have participated in its planning, design and execution, as well as in the interpretation of the results. They also critically reviewed the paper, approved its final version and agreed with its publication.

- No signature responsible for the work has been omitted and the criteria of Scientific Authorization are satisfied.

- The results of this Article have been interpreted objectively. Any results contrary to the point of view of those who sign are exposed and discussed in the Article.

## Copyright and Access

The publication of this Article supposes the transfer of the copyright to ECORFAN-Mexico, SC in its Holding Republic of Peru for its Journal of Innovative Engineering, which reserves the right to distribute on the Web the published version of the Article and the making available of the Article in This format supposes for its Authors the fulfilment of what is established in the Law of Science and Technology of the United Mexican States, regarding the obligation to allow access to the results of Scientific Research.

Article Title:

| Name and Surnames of the Contact Author and the Coauthors | Signature |
|---|---|
| 1. | |
| 2. | |
| 3. | |
| 4. | |

## Principles of Ethics and Declaration of Solution to Editorial Conflicts

### Editor Responsibilities

The Publisher undertakes to guarantee the confidentiality of the evaluation process, it may not disclose to the Arbitrators the identity of the Authors, nor may it reveal the identity of the Arbitrators at any time.

The Editor assumes the responsibility to properly inform the Author of the stage of the editorial process in which the text is sent, as well as the resolutions of Double-Blind Review.

The Editor should evaluate manuscripts and their intellectual content without distinction of race, gender, sexual orientation, religious beliefs, ethnicity, nationality, or the political philosophy of the Authors.

The Editor and his editing team of ECORFAN® Holdings will not disclose any information about Articles submitted to anyone other than the corresponding Author.

The Editor should make fair and impartial decisions and ensure a fair Double-Blind Review.

### Responsibilities of the Editorial Board

The description of the peer review processes is made known by the Editorial Board in order that the Authors know what the evaluation criteria are and will always be willing to justify any controversy in the evaluation process. In case of Plagiarism Detection to the Article the Committee notifies the Authors for Violation to the Right of Scientific, Technological and Innovation Authorization.

### Responsibilities of the Arbitration Committee

The Arbitrators undertake to notify about any unethical conduct by the Authors and to indicate all the information that may be reason to reject the publication of the Articles. In addition, they must undertake to keep confidential information related to the Articles they evaluate.

Any manuscript received for your arbitration must be treated as confidential, should not be displayed or discussed with other experts, except with the permission of the Editor.

The Arbitrators must be conducted objectively, any personal criticism of the Author is inappropriate.

The Arbitrators must express their points of view with clarity and with valid arguments that contribute to the Scientific, Technological and Innovation of the Author.

The Arbitrators should not evaluate manuscripts in which they have conflicts of interest and have been notified to the Editor before submitting the Article for Double-Blind Review.

**Responsibilities of the Authors**

Authors must guarantee that their articles are the product of their original work and that the data has been obtained ethically.

Authors must ensure that they have not been previously published or that they are not considered in another serial publication.

Authors must strictly follow the rules for the publication of Defined Articles by the Editorial Board.

The authors have requested that the text in all its forms be an unethical editorial behavior and is unacceptable, consequently, any manuscript that incurs in plagiarism is eliminated and not considered for publication.

Authors should cite publications that have been influential in the nature of the Article submitted to arbitration.

**Information services**

**Indexation - Bases and Repositories**

LATINDEX (Scientific Journals of Latin America, Spain and Portugal)
EBSCO (Research Database - EBSCO Industries)
RESEARCH GATE (Germany)
GOOGLE SCHOLAR (Citation indices-Google)
MENDELEY (Bibliographic References Manager)
HISPANA (Information and Bibliographic Orientation-Spain)

**Publishing Services**

Citation and Index Identification H
Management of Originality Format and Authorization
Testing Article with PLAGSCAN
Article Evaluation
Certificate of Double-Blind Review
Article Edition
Web layout
Indexing and Repository
ArticleTranslation
Article Publication
Certificate of Article
Service Billing

**Editorial Policy and Management**

1047 La Raza Avenue -Santa Ana, Cusco-Peru. Phones: +52 1 55 6159 2296, +52 1 55 1260 0355, +52 1 55 6034 9181; Email: contact@ecorfan.org www.ecorfan.org

# Journal of Innovative Engineering




2523 6873
ISSN 2523 - 6873


www.ecorfan.org